Hint for a Minimal Interaction Length in e#e# → yy Annihilation in Total Cross Section of Center-of-Mass Energies 55-207 GeV

Author(s):
Chen, Yutao; Liu, Minghui; Ulbricht, Jürgen

Publication date:
2024

Permanent link:
https://doi.org/10.3929/ethz-b-000670460

Originally published in:
Advances in High Energy Physics 2024, https://doi.org/10.1155/2024/9755683

Hindawi
Advances in High Energy Physics
Volume 2024, Article ID 9755683, 23 pages
https://doi.org/10.1155/2024/9755683

Research Article

Hint for a Minimal Interaction Length in $e^+e^- \longrightarrow \gamma\gamma$ Annihilation in Total Cross Section of Center-of-Mass Energies 55-207 GeV

Yutao Chen,[1] Minghui Liu ,[1] and Jürgen Ulbricht[2]

[1]*Department of Modern Physics, University of Science and Technology of China, Jinzhai Road 96, Hefei, Anhui 230026, China*
[2]*Swiss Institute of Technology ETH Zurich, CH-8093 Zurich, Switzerland*

Correspondence should be addressed to Minghui Liu; hepglmh@ustc.edu.cn

Received 17 November 2022; Revised 16 January 2024; Accepted 8 March 2024; Published 10 April 2024

Academic Editor: Luciano Petruzziello

The measurements of the total cross section of the $e^+e^- \longrightarrow \gamma\gamma(\gamma)$ reaction from the VENUS, TOPAS, OPAL, DELPHI, ALEPH, and L3 collaborations, collected between 1989 and 2003, are used to perform a χ^2 test to validate the current quantum electrodynamics (QED) theory and search for possible deviations with the direct contact term annihilation. By observing a deviation from the QED predictions on the total cross section of the $e^+e^- \longrightarrow \gamma\gamma(\gamma)$ reaction above $\sqrt{s} = 180.0$ GeV, a non-QED direct contact term is introduced following the dimension 6 effective theory to explain the deviation. In the non-QED direct contact term, a threshold energy scale Λ is included and explained to the finite interaction length in direct contact term and in consequence the size of the electron involved in the annihilation area. The experimental data of the total cross section is compared to the QED cross section by a χ^2 test, which gives a best fit of the Λ to be 1576 ± 202 GeV, corresponding to a finite interaction length of $r_e = (1.25 \pm 0.16) \times 10^{-17}$ (cm). In the direct contact term annihilation, this interaction length is a measure of the size of an electron r_e. By combining all the data results from the mentioned collaborations, we have at least 2 to 3 times more statistics than every single experiment at high $\sqrt{s}$ region. This induces the best precision on r_e compared to the previous measurements.

1. Introduction

The Standard Model (SM) of particle physics is the theory describing three of the four known fundamental forces (the electromagnetic (QED), weak, and strong interactions). After the discovery of the three families of fundamental particles, the gluons, photon, Z-boson, and W-boson, the discovery of Higgs in 2012 established the last cornerstone of the SM. Missing so far is the unification between the SM and the fourth interaction, the gravitation. It is for this reason essential to investigate deviations of the SM. All the three fundamental forces have a definite interaction length. In particular, the QED has an infinite interaction length. In this paper, we search for minimal interaction length. A minimal interaction length would be an indication of a deviation from the QED. The concept of a minimal interaction length suggested by path-integral quantisation [1], string theory [2, 3], black hole physics [4], and quantum gravity [5–7] has been introduced into quantum mechanics and quantum field theory through generalized uncertainty principle [8, 9] which restricts an accuracy of Δl in measuring a particle position by a certain finite minimal length scale l_m related to maximum resolution [10–12] (for a review, see [13]). In gravity, the limiting quantum length is the Planck length $l_P = \sqrt{\hbar G/c^3} = 1.6 \times 10^{-33}$ cm, the related energy scale $M_P \simeq 10^{16}$ TeV. However, gravitational effects have only been tested up to 1 TeV scale [14] which corresponds to $l_m \simeq 10^{-17}$ cm [15]; therefore, minimal length could be in principle found within the range l_P and l_m [15]. In models with extra dimensions, the Planck length can be reduced to $1/M_f$ with $M_f \simeq 1$ TeV, which results in modification of the cross sections of basic scattering processes $e^+e^- \longrightarrow \mu^+\mu^-$, $e^+e^- \longrightarrow \tau^+\tau^-$ ([16] and references therein).

In this paper, we summarize the results of investigating experimental data on the annihilation reaction

$e^+e^- \longrightarrow \gamma\gamma(\gamma)$ motivated by the search for manifestation of the non-point-like behavior of fundamental particles.

In a first approach, the question of the intrinsic structure of a charged spinning particle like an electron has been discussed in the literature since its discovery by Thomson in 1897. In quantum field theory, a particle is assumed to be point-like, and classical models of point-like spinning particles describe them by various generalizations of the classical Lagrangian $(-mc\sqrt{\dot{x}\dot{x}})$ [17–31]. Another type of point-like model [32–42] goes back to Schrödinger's suggestion that the electron spin can be related to its zitterbewegung motion [43]. The development of this approach ends today in the excellent experimental tested Standard Model of particle physics. The model is described by three families of point-like particles. The point-like structure of the fundamental particle with rest mass $m > 0$ requests an unnatural density $\rho \longrightarrow \infty$. The SM is a stand-alone model which does not include the fourth interaction, the gravity.

A second approach works with extended particle models. Early electron models based on the concept of an extended electron, proposed by Abraham and Lorentz more than a hundred years ago [44, 45], encountered the problem of preventing an electron from flying apart under the Coulomb repulsion. Theories based on geometrical assumption about the "shape" or distribution of a charge density were compelling to introduce cohesive forces of nonelectromagnetic origin (the Poincaré stress) [46]. A new review of models is discussed in [47]. In this paper, we apply this model [47]. To find evidence for an extended particle picture, we used available data from experiments performed to search for a non-point-like behavior, which focuses on characteristic energy scales related to characteristic length of interaction region in reference [48–54]. Experimental limits on the size of a lepton in reference [48–52] appear to be much less than its classical radius which suggests the existence of a relatively small characteristic length scale related to gravity in reference [48–52]. A non-point-like behavior of fundamental particles would open a window to the fundamental problem in physics beyond the SM for unification between the SM and the gravity in terms of general relativity. The different concepts of extended particle models discussed in reference [44–47], in particular, the paper "Image of the Electron Suggested by Nonlinear Electrodynamics coupled to Gravity" [7] and "Gravity vs. quantum theory: is electron really point like?" [47] in connection with the generalized uncertainty principle [8, 9], show an example of a path to include the gravity in physics beyond the SM. Essential is that the inclusion of gravity in the different models allows a transition between the SM and the general relativity. The unnatural density $\rho \longrightarrow \infty$ of the fundamental particle would disappear. To confirm the theoretical approach of a non-point-like behavior of fundamental particles, it is essential in an experiment to detect a minimal interaction length.

To investigate the pure electromagnetic interaction $e^+e^- \longrightarrow \gamma\gamma(\gamma)$ using differential cross data from VENUS, TOPAS, ALEPH, DELPHI, L3, and OPAL sets the limit on a maximal resolution at scale $E = 1.253\,\text{TeV}$ by the character length $l_e \simeq 1.57 \times 10^{-17}\,\text{cm}$ with a 5σ significance

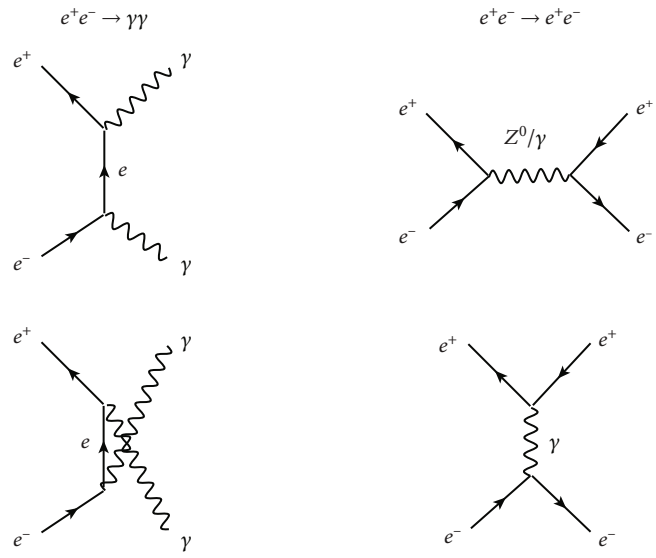

Figure 1: Lowest order $e^+e^- \longrightarrow \gamma\gamma$ and $e^+e^- \longrightarrow e^+e^-$ reactions. The reaction $e^+e^- \longrightarrow \gamma\gamma$ proceeds via the t- and u-channels. The Bhabha $e^+e^- \longrightarrow e^+e^-$ channel proceeds via the s- and t-channels.

[53, 54]. An earlier report set a 2.6σ on an axial-vector contact interaction in the data on $e^+e^- \longrightarrow e^+e^-(\gamma)$ at center-of-mass energies 192-208 GeV [55].

The available data from the e^+e^- accelerators favor two experiments to test the finite interaction length the $e^+e^- \longrightarrow \gamma\gamma$ and $e^+e^- \longrightarrow e^+e^-$ reactions. Both reactions are shown in Figure 1.

The QED reaction $e^+e^- \longrightarrow \gamma\gamma$ is testing the behavior of the electrodynamics long-range force of the e^+e^- reaction. The two γ's in the final state of the reaction $e^+e^- \longrightarrow \gamma\gamma$ are indistinguishable. The reaction performs for this reason via the t- and u-channels. The s-channel is forbidden, by the law of angular momentum conservation. The two γ's in the final state are left-handed and right-handed polarized. They couple to total spin zero. Under these circumstances, the s-channel with spin one for γ and Z^0 is highly suppressed.

The Bhabha reaction $e^+e^- \longrightarrow e^+e^-$ is not only sensitive to the long-range force of the electromagnetic e^+e^- reaction, in addition via the Z^0 also to the short-range force of the electroweak interaction. The reaction proceeds, via scattering in the s-channel and t-channel. The e^+ and e^- in the initial state and final state are identical. The gammas in the final state of the $e^+e^- \longrightarrow \gamma\gamma$ reaction disappear. The high charge sensitivity of the involved detectors allows to suppress the background $e^+e^- \longrightarrow e^+e^-$ reaction, even under the circumstances that at the Z^0 pole, the total cross section of the $e^+e^- \longrightarrow e^+e^-$ reaction is a factor two bigger as the total cross section of the $e^+e^- \longrightarrow \gamma\gamma$ reaction.

After the commissioning of the high energy e^+e^- accelerators 1986 TRISTAN at KEK, the VENUS collaboration (1989) initiated the first experiments at $\sqrt{s} = 55\,\text{GeV}$ to investigate the total and differential cross section of the $e^+e^- \longrightarrow \gamma\gamma$ reaction. The experiments continued until LEP was closed 2000 at $\sqrt{s} = 207\,\text{GeV}$.

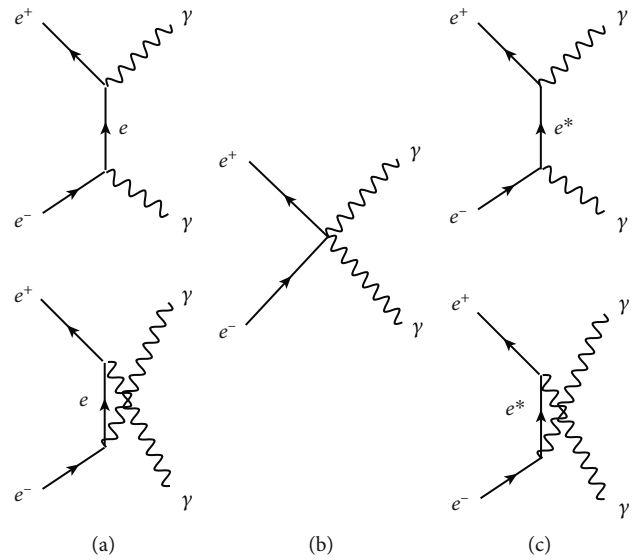

Figure 2: Lowest order Feynman diagrams of $e^+e^- \longrightarrow \gamma\gamma$ reaction: (a) QED, (b) contact interaction, and (c) excited electron exchange.

In detail, the reaction was investigated by the VENUS collaboration [56] from energies $\sqrt{s} = 55\,\text{GeV}$ to $57\,\text{GeV}$, OPAL collaboration [57] at the Z^0 pole at $\sqrt{s} = 91\,\text{GeV}$, TOPAS collaboration [58] at $\sqrt{s} = 57.6\,\text{GeV}$, ALEPH collaboration [59] at the Z^0 pole at $\sqrt{s} = 91.0\,\text{GeV}$, DELPHI collaboration [60–62] from 1994 to 2000 at energies $\sqrt{s} = 91.25\,\text{GeV}$ to $202\,\text{GeV}$, L3 collaboration [63] from 1991 to 1993 at the Z^0 pole range from $\sqrt{s} = 88.5\,\text{GeV}$ to $93.7\,\text{GeV}$, L3 collaboration [64] from $\sqrt{s} = 183\,\text{GeV}$ to $207\,\text{GeV}$, and OPAL collaboration [65] from $\sqrt{s} = 181\,\text{GeV}$ to $209\,\text{GeV}$.

The experimental data of the differential cross section of these six collaborations from $\sqrt{s} = 55\,\text{GeV}$ to $207\,\text{GeV}$ are compared to the theoretical predicted QED differential cross section. Possible deviations from QED were studied in terms of contact interaction and excited electron exchange shown in Figure 2.

The deviation to the QED reaction is visible in the angular distribution of the gammas from the experiment to the QED theory and in the experimental total cross section data to the QED. It is necessary to perform, for example, a χ^2 test or similar statistical tests, to search in the test for a minimum or limit for a scale parameter Λ (GeV). This parameter finally allows to define a finite radius of the electron or the mass of an excited heavy electron. It is important to notice that a signal of deviation from QED is not visible in new final state particles like for the HIGGS search; it is hidden only in the angular distribution of the differential cross section and in the energy dependence of the total cross section to the QED values.

All the collaborations search for bounds on effective interactions from the reaction $e^+e^- \longrightarrow \gamma\gamma$, for example, [66]. Cutoff parameter Λ is used to set mass scales of different dimensional interactions. Data of differential cross section are used to set limits on compositeness scales Λ_+ and Λ_- in the direct contact interaction of the diagram shown in Figure 2(b) and search for excited electrons m_{e^*} in the t- and u-channels of the diagram shown in Figure 2(c). For example, the L3 collaboration published four papers (1992, 1996, 1997, and 2000) and set (1992) [67–70] limits on $\Lambda_+ > 139\,\text{GeV}$ and $\Lambda_- > 108\,\text{GeV}$ and a limit on the mass of an excited electron to $m_{e^*} > 127\,\text{GeV}$.

1.1. Outline of This Paper. The VENUS, TOPAS, OPAL, DELPHI, L3, and ALEPH collaborations used the differential cross section of the $e^+e^- \longrightarrow \gamma\gamma$ reaction to search for a deviation from QED. This was performed for certain energy ranges and luminosities.

Even all the mentioned experiments above are closed and there is no more new data come in, it is possible to combine all these data results from each single experiment and perform a global χ^2 test. This combination can give us 2-3 times more data in high $\sqrt{s}$ region, e.g., $\sqrt{s} > 180\,\text{GeV}$, thus yielding much better results. It is also important to mention that the scale parameter Λ allows to define a finite radius of electrons r_e through the generalized uncertainty principle as discussed in Section 2.5. The limits on r_e are not presented in any of the previous single experiment result. In this study, we motived to analyze the combined data results from all the 6 experiments and give the first limits on r_e through the $e^+e^- \longrightarrow \gamma\gamma$ process.

We have performed a global χ^2 FIT, using the differential data from these six research projects to investigate Λ_+, Λ_-, and m_{e^*} for energies from $\sqrt{s} = 55\,\text{GeV}$ to $207\,\text{GeV}$ including the associated luminosities [51, 54, 71]. That analysis allowed to set an approximately $5 \times \sigma$ limit on the finite size of the electron $r = (1.57 \pm 0.28) \times 10^{-17}$ (cm) and on the mass of an exited electron of $m_{e^*} = 308 \pm 56$ (GeV). The deviation in the differential experimental cross section from the QED values of approximately 4% was only visible in the fit results but not direct in the comparison of the experimental and theoretical QED cross section.

The aim of this instigation is to prove in a χ^2 fit that the use of only the total cross section of all these data implies a similar result. First, it is necessary to discuss the

theoretical framework of the calculation of the total QED cross section, in particular, the fact that an analytic precise QED cross section must be calculated via a Monte Carlo program. Second, as no total cross section for the QED $e^+e^- \longrightarrow \gamma\gamma$ reaction from $\sqrt{s} = 55\,\text{GeV}$ to $207\,\text{GeV}$ exists, we introduced a model for a total cross section using the data from the 6 collaborations. Including this information, it is possible to perform a total χ^2 fit with all data. Finally, it is possible to discuss the results.

2. Theoretical Framework

To test the point structure of the electron, request a high precision of the theoretical QED calculation of the differential and total cross section of the $e^+e^- \longrightarrow \gamma\gamma$ reaction.

The interactions of particles are dictated by symmetry principles of local gauge invariance and conserved physical quantities. Mathematically, the Lagrangian formalism is used to connect symmetries and conservation laws.

The Euler Lagrange equation is used to describe a free particle with spin 1/2. The minimum of the action path integral is the Lagrangian density of the Dirac equation.

$$\mathscr{L}_{\text{Dirac}} = \bar{\Psi}\left(i\gamma^\mu \partial_\mu - m\right)\Psi, \tag{1}$$

where Ψ is the fermion field, $\bar{\Psi} \equiv \Psi^+\gamma^0$ is its adjoint spinor, γ^μ is the gamma matrices, $\partial^\mu = \partial/\partial x_\mu$ is the covariant derivative, and m is the mass of the particle.

A particle with interaction is described by the local gauge invariance QED Lagrangian function in

$$\mathscr{L}_{\text{QED}} = \bar{\Psi}\left(i\gamma^\mu \partial_\mu - m\right)\Psi + e\bar{\Psi}\gamma^\mu A_\mu \Psi - \frac{1}{4} F_{\mu\nu}F^{\mu\nu}, \tag{2}$$

where A_μ is the gauge field, the mass $m_A = m_\gamma = 0$, e is the charge of the electron, $e\bar{\Psi}\gamma^\mu A_\mu \Psi$ is the interaction term, and $F_{\mu\nu} = \partial_\mu A_\nu - \partial_\nu A_\mu$.

2.1. The Lowest Order Cross Section of $e^+e^- \longrightarrow \gamma\gamma$. The interaction term of the QED Lagrangian allows to calculate the lower case Born cross section of the $e^+e^- \longrightarrow \gamma\gamma$ reaction. The mathematical formalism uses the M matrix of

$$M_{fi} = -e \int \bar{\Psi}\gamma^\mu \Psi A_\mu d^4x, \tag{3}$$

where f stands for the final state and i stands for the initial state. The derivation of the differential cross section uses the square of the M matrix, including the t- and u-channels of the Feynman graphs of Figure 2(a) and neglecting the electron mass $m_e \approx 0$ for high energies.

$$\frac{d\sigma_0}{d\Omega} = \frac{S}{64\pi^2 s}\frac{p_f}{p_i}|M|^2 = \frac{\alpha^2}{s}\frac{1 + cos^2(\theta)}{k - cos^2(\theta)}. \tag{4}$$

$S = 1/2$ is a statistical factor, $\sqrt{s}$ is the center-of-mass energy, the momentum $p_f = p_i$, $k = E_{e^+}/|\vec{p}_{e^+}| \simeq 1$ for high energies E_{e^+}, and $\alpha = e^2/4\pi$. The angle θ is the photon-scattering angle with respect to the e^+e^- beam axis.

The total Born cross section is the integral over the angle θ and the azimuth angle ϕ.

$$\sigma^0 = \frac{1}{2!}\frac{\alpha^2}{s}\int_0^{2\pi} d\phi \int_{-1}^{+1} \frac{1 + \cos^2\theta}{k - \cos^2\theta} d(\cos\theta) = \frac{2\pi\alpha^2}{s}\left(\ln\left(\frac{s}{m_e^2}\right) - 1\right). \tag{5}$$

The precision of the Born cross sections is absolutely not sufficient to search for non-point-like behavior of the electron in a χ^2 fit of the $e^+e^- \longrightarrow \gamma\gamma(\gamma)$ reaction.

2.2. Radiative Corrections of the QED $e^+e^- \longrightarrow \gamma\gamma(\gamma)$ Cross Section. All 6 collaborations used radiative corrections of the QED $e^+e^- \longrightarrow \gamma\gamma(\gamma)$ cross section for virtual, soft, and hard photons [54, 72, 73]. In total, 22 corrections are implemented [73, 74].

The first set of eight virtual photon corrections is shown in the Feynman graphs of Figure 3 [75].

The second set of four soft real photon initial state corrections, including the six hard photon corrections, is shown in the Feynman graphs of Figure 4 [75].

2.3. The $e^+e^- \longrightarrow \gamma\gamma(\gamma)$ Total Cross Section for Hard Core and Soft Core Radiative Corrections. The differential cross section for the soft- and hard-Bremsstrahlung process is not analytically known. The corrections of the Feynman diagrams from Figures 3 and 4 are calculated by numerical simulations. The details of the differential cross section for the numerical approach are shown in Appendix A and B.

An analytic equation of total integrated cross section, adding the $e^+e^- \longrightarrow \gamma\gamma$ plus $e^+e^- \longrightarrow \gamma\gamma(\gamma)$ reactions can be calculated with (6) and (7).

$$\sigma_{\text{tot}} = \sigma(2\gamma) + \sigma(3\gamma), \tag{6}$$

$$= \sigma^0 + \frac{2\alpha^3}{s}\left[\frac{4}{3}\nu^3 - \nu^2 + \left(\frac{2}{3}\pi^2 - 2\right)\nu + 2 - \frac{1}{12}\pi^2\right]. \tag{7}$$

The parameter ν is as a function of the mass m_e of the electron and the $\sqrt{s}$.

$$\nu = \frac{1}{2}\ln\left(\frac{s}{m_e^2}\right). \tag{8}$$

2.4. The Numerical Calculation of the $e^+e^- \longrightarrow \gamma\gamma(\gamma)$ Cross Sections. For practical reasons, the differential and total cross sections were used from the numerical calculation for the χ^2 fit.

2.4.1. The Calculation of the $e^+e^- \longrightarrow \gamma\gamma(\gamma)$ Differential Cross Sections. The 6 collaborations under discussion used an event generator [73, 74] for the reaction $e^+e^- \longrightarrow \gamma\gamma(\gamma)$.

$$e^+(p_+) + e^-(p_-) \longrightarrow \gamma(k_1) + \gamma(k_2) + \gamma(k_3). \tag{9}$$

The lowest order differential cross section $(d\sigma/d\Omega)_{\text{Born}}$ is

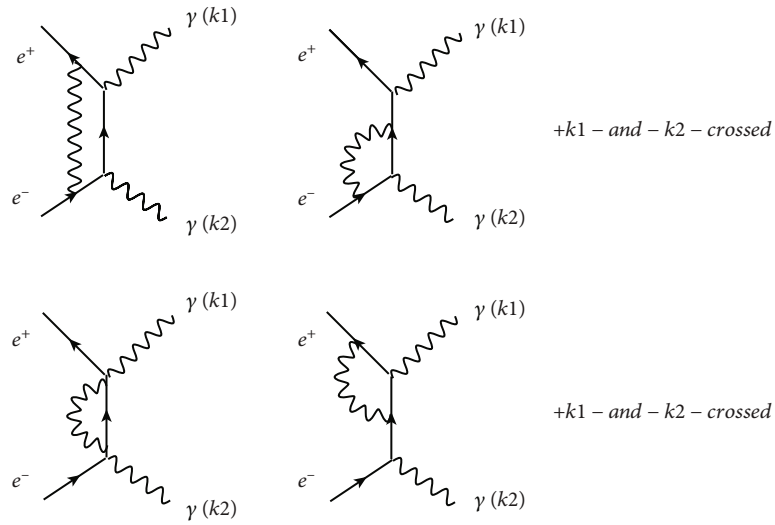

Figure 3: Third order of eight virtual photon corrections Feynman graphs of the $e^+e^- \longrightarrow \gamma\gamma(\gamma)$ reaction.

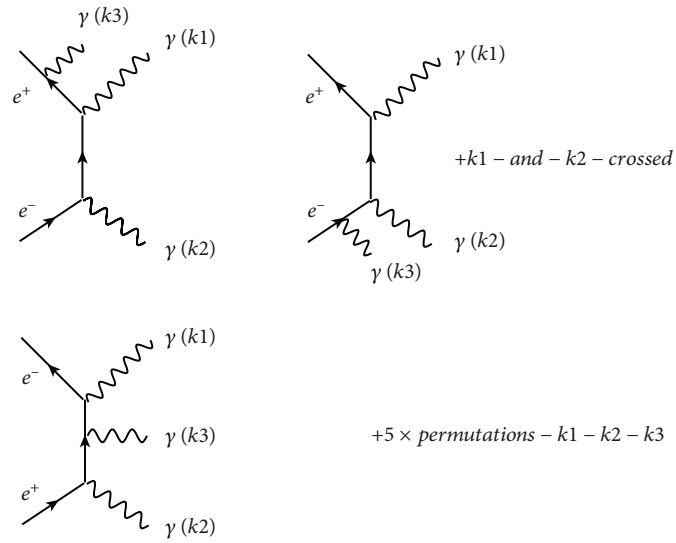

Figure 4: Third-order Feynman graphs of the $e^+e^- \longrightarrow \gamma\gamma(\gamma)$ reaction, four soft initial photon corrections, and six hard photon corrections.

corrected numerically by adding the higher order correction of Figures 3 and 4 to $O(\alpha^3)$ in

$$\left(\frac{d\sigma}{d\Omega}\right)_{\alpha^3} = \left(\frac{d\sigma}{d\Omega}\right)_{\text{Born}} (1 + \delta_{\text{virtual}} + \delta_{\text{soft}} + \delta_{\text{hard}}), \quad (10)$$

where δ_{virtual} is the virtual correction and δ_{soft} and δ_{hard} are the soft- and hard-Bremsstrahlung corrections.

If the energy of the photons from initial state radiation (soft Bremsstrahlung) are too small to be detected, the reaction can be treated as 2-photon final state. This is valid if the parameter $k_3/|p_+| = k_0 << 1$ of the e^+e^- reaction is fulfilled (11).

$$e^+(p_+) + e^-(p_-) \longrightarrow \gamma(k_1) + \gamma(k_2)). \quad (11)$$

For the third-order differential cross section, the program generates three γ events sorted after the energies $E_{\gamma 1} \geq E_{\gamma 2} \geq E_{\gamma 3}$, with the correct mixture for soft $k_3/|p_1| = k_0 \ll 1$ and hard QED corrections shown in Figures 3 and 4. The angle β between the $E_{\gamma 1}$ and $E_{\gamma 2}$ event $\beta_{\min} < \beta < \beta_{\max}$ is connected to the scattering angle θ by $|\cos\theta|$.

The differential cross section $(d\sigma/d\Omega)_i$ at an angle θ, an energy E_{tot}, and an angle bin width $\Delta(|\cos\theta|)$ can be expressed with

$$\left(\frac{d\sigma}{d\Omega}\right)_i = \frac{1}{2\pi\Delta(|\cos\theta|)}\sigma_{\text{tot}}\frac{N_i}{N}. \quad (12)$$

The scattering angle is $|\cos\theta| = (|\cos\theta_1| + |\cos\theta_2|)/2$, where θ_1 is the scattering angle of $E_{\gamma 1}$ and θ_2 is the scattering angle of $E_{\gamma 2}$, N_i is the number of events in an angle bin width $\Delta(|\cos\theta|)$, and N is the total amount of events used

in the generator. The Monte Carlo generator together with (12) is used to calculate distributions of differential cross sections as a function of $|\cos\theta|$ including the five discussed parameters.

In the past, the Monte Carlo generator [73, 74] was used from all 6 collaborations, to generate the QED cross section of the $e^+e^- \longrightarrow \gamma\gamma(\gamma)$ reaction. Our interest is focused on a new Monte Carlo generator BabaYaga@nlo [76]. To use the BabaYaga QED generator, request a comparison of QED cross section data from both generators. The new generator implements the same radiative corrections of Figures 3 and 4. To generate BabaYaga@nlo $e^+e^- \longrightarrow \gamma\gamma(\gamma)$ events, the following seven parameters are used:

$$\begin{aligned}
p_{11} &= \text{final} - \gamma - \text{state} = \text{gg},\\
p_{22} &= \sqrt{S} - \text{ecms} - \text{energy (GeV)},\\
p_{33} &= \text{minimum} - \text{angle} - \theta_{\min} - \text{thmin (deg)},\\
p_{44} &= \text{maximum} - \text{angle} - \theta_{\max} - th \text{ max (deg)},\\
p_{55} &= \text{accollinear} - \text{angle} - \text{acoll.} - \beta \text{ (deg)},\\
p_{66} &= \text{minimum} - \text{energy} - e \text{ min (GeV)},\\
p_{77} &= \text{number} - \text{generating} - \text{events} = N.
\end{aligned} \tag{13}$$

To perform a χ^2 fit for a finite size of the electron, an analytical expression for the differential cross section (12) is needed. The angular distribution of the differential cross section (12) is fitted by a χ^2 fit using a polynomial with 6 parameters p_1 to p_6 shown in (14).

$$\left(\frac{d\sigma}{d\Omega}\right)_{QED} = \left(\frac{d\sigma}{d\Omega}\right)_{Born} \times \left(1 + p_1 + p_2 e^{-x^{1.2}/2p_3^2} + p_4 x + p_5 x^2 + p_6 x^3\right)\Big|_{x=|\cos\theta|}. \tag{14}$$

To calculate cross sections for different detectors, it is necessary for the calculation of the QED cross sections to regard the various parameters how every detector is able to measure events. We normalize all cross section measurements and calculation of the QED cross section to the L3 parameters [64].

$$\begin{aligned}
p_{11} &= \text{final} - \gamma - \text{state} = \text{gg},\\
p_{22} &= \sqrt{S} - \text{ecms} - \text{energy (GeV)},\\
p_{33} &= \text{minimum} - \text{angle} - \theta_{\min} - \text{thmin} = 16.0 \text{ (deg)},\\
p_{44} &= \text{maximum} - \text{angle} - \theta_{\max} - \text{thmax} = 164.0 \text{ (deg)},\\
p_{55} &= \text{accollinear} - \text{angle} - \text{acoll.} - \beta = 90.0 \text{ (deg)},\\
p_{66} &= \text{minimum} - \text{energy} - e \text{ min} = 0.48 \text{ (GeV)},\\
p_{77} &= \text{number} - \text{generating} - \text{events} = N = 100000.
\end{aligned} \tag{15}$$

Considering the experimental data of the ratio of the total measured cross section divided by the total QED cross section $R = \sigma(\text{exp})/\sigma(\text{QED})$ of the L3 collaboration [64] shown in Figure 2, a small deviation from the QED ratio R from 90 GeV to 207 GeV is visible. To test the QED deviation as a function of $\sqrt{s}$, we performed two sets of χ^2 tests: one set from 55 GeV to 207 GeV with 17 energy points and the other set from 91.2 GeV to 200 GeV with 7 energy points.

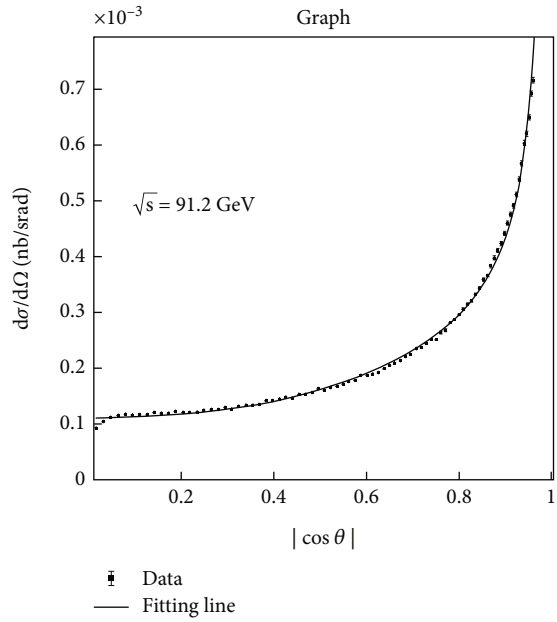

FIGURE 5: Differential QED BabaYaga cross section of the $e^+e^- \longrightarrow \gamma\gamma(\gamma)$ reactions at $\sqrt{s} = 91.2$ GeV. It is normalized to the parameters of L3. Points are the cross section, and black line is the fit.

Including the parameters of (15), it is possible to calculate and fit all 17 angular distributions of the energies under request from $\sqrt{s} = 55$ GeV to 207 GeV. The 6 fit parameters p_1 to p_6 (14) are summarized in Table 8 (upper part) in Appendix C. The same parameters for 7 $\sqrt{s}$ energies from $\sqrt{s} = 91.2$ GeV to 200 GeV of the generator [73, 74] are summarized in Table 8 (lower part) in Appendix C.

For an example at $\sqrt{s} = 91.2$ GeV, the differential QED cross section fitted to (14) is shown in Figure 5.

Including the fit parameters from Table 8 together with (16), it is possible to calculate the total QED BabaYaga cross section from $\sqrt{s} = 55$ GeV to 207 GeV in Figure 6. The points are the cross section.

$$\sigma_{\text{tot}}(\text{QED}) = \int_{\theta=16.0^\circ}^{\theta=164.0^\circ} \left(\frac{d\sigma}{d\Omega}\right)_{\text{QED}} d|\cos\theta|. \tag{16}$$

The red line is a fit using (17) and (18) to form an analytic expression to the total QED cross section. The two fitting parameters are $a = -3.4 \times 10^4$ and $b = 4.8 \times 10^7$.

$$\sigma(\text{QED})_{\text{tot}}^{\text{L3}} = \sigma(2\gamma) + \text{korr} \cdot \sigma(3\gamma), \tag{17}$$

$$\text{korr} = a \cdot \sqrt{s} + b. \tag{18}$$

To compare all the experimental data to the QED data, the six collaboration used the Monte Carlo QED

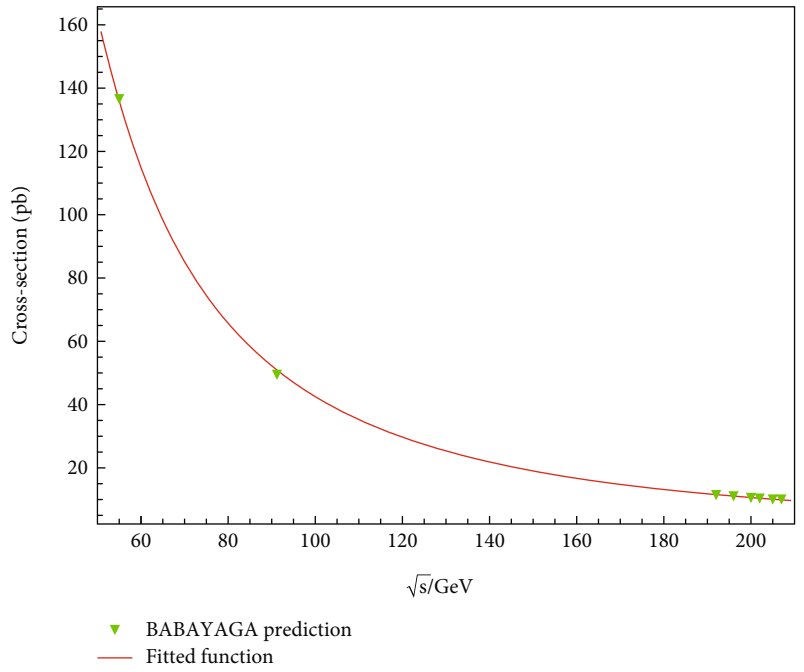

FIGURE 6: Total QED BabaYaga cross section of the $e^+e^- \longrightarrow \gamma\gamma(\gamma)$ reactions. The points are the cross section, and the red line is a fit to this points.

generator [73, 74]; in this analysis, we used the generator BabaYaga@nlo [76]. For this reason, it was necessary to search for deviation between both QED generators.

The total cross section from the Monte Carlo QED generator [73, 74] and the [76] is in the range of the statistical error bar the same. At energies between $\sqrt{s} = 91.0$ GeV and 207.0 GeV, the middle value of [73, 74] is $\sigma_{\text{tot}}(\text{QED}) = 16.2$ (pb) and [76] is $\sigma_{\text{tot}}(\text{QED}) = 16.1$ (pb), a total deviation of $\Delta\sigma_{\text{tot}}(\text{QED}) = -0.1$ (pb). This is approximately the statistical error of the QED generator [73, 74] of $\Delta\sigma_{\text{tot}}(\text{QED}) = \pm 0.1$ (pb). The total cross section $\sigma_{\text{tot}}(\text{QED})$ of [76] above $\sqrt{s} = 91.0$ GeV is approximately 0.9% smaller as in [73, 74].

2.5. Deviations from QED. If the QED is a fundamental theory, the experimental parameters of the $e^+e^- \longrightarrow \gamma\gamma(\gamma)$ reaction should be correctly calculated by the Monde Carlo generator [73, 74] or [76] up to the grand unification scale. All collaborations [56] to [67–70] investigated deviations from the QED $e^+e^- \longrightarrow \gamma\gamma(\gamma)$ reaction from $\sqrt{s} = 55$ GeV up to $\sqrt{s} = 207$ GeV. New non-QED phenomenon could become visible at high energy scales and may be below the grand unification scale. An energy scale characterized by a cutoff parameter Λ (GeV) can be used as a threshold point for a QED breakdown and for the underlying new physics. Different models are discussed in [77–81]. Deviations from QED with the reaction $e^+e^- \longrightarrow \gamma\gamma(\gamma)$ [82–86] are investigated in a program initiated between 1991 and 2020 by the Swiss Federal Institute of Technology in Zurich (ETHZ) and USTC Hefei (University of Science and Technology of China). In this paper, we focus on a model of finite size of an interaction length in the $e^+e^- \longrightarrow \gamma\gamma(\gamma)$ reaction.

2.5.1. In the Direct Contact Term Annihilation, a Finite Interaction Length Is a Measure for the Size of the Electron. The QED differential and total cross sections of the $e^+e^- \longrightarrow \gamma\gamma(\gamma)$ reaction are calculated under the condition that the electron is point-like, without limited interaction length and coupled to the vacuum as shown in Figures 3 and 4. So far, no experiments exist to test, in particular, the non-limited interaction length of the electron up to the Planck scale. If at a certain energy scale Λ between $0 < \Lambda < M_P$ in the $e^+e^- \longrightarrow \gamma\gamma(\gamma)$ reaction, a finite interaction length appears, this Λ defines a size of an object where the annihilation occurs. It is possible to calculate the size of the object via the generalized uncertainty principle [10–12] or via the electromagnetic energy E and wavelength λ [87] of the light that the object submits.

It is well known that the wavelength λ of the gammas must be smaller or equal to the size of the interaction area. If the energy Λ of the size of the interaction area is known, the frequency ν of the gammas is known via $\Lambda = E = \hbar \times \nu$. This frequency ν is connected to the size of the object via the wavelength λ to the equation $\nu \times \lambda = c$. The energy scale Λ defines under these circumstances the size of the interaction area and in consequence the size of the electron involved in the annihilation area.

It is possible to construct several effective Lagrangians containing nonstandard γe^+e^- or $\gamma\gamma e^+e^-$ couplings which are $U(1)_{\text{em}}$ gauge invariant and only differ in their dimensions [77–81]. In the lowest order effective Lagrangian, this reaction contains operators of dimension 6, 7, and 8 [66]. In the further discussion, we concentrate on the simplest operator of dimension 6, with the effective Lagrangian of

$$\mathscr{L}_6 = i\bar{\Psi}\gamma_\mu\left(\vec{D}_\nu\Psi\right)\left(g_6 F^{\mu\nu} + \tilde{g}_6\tilde{F}^{\mu\nu}\right). \tag{19}$$

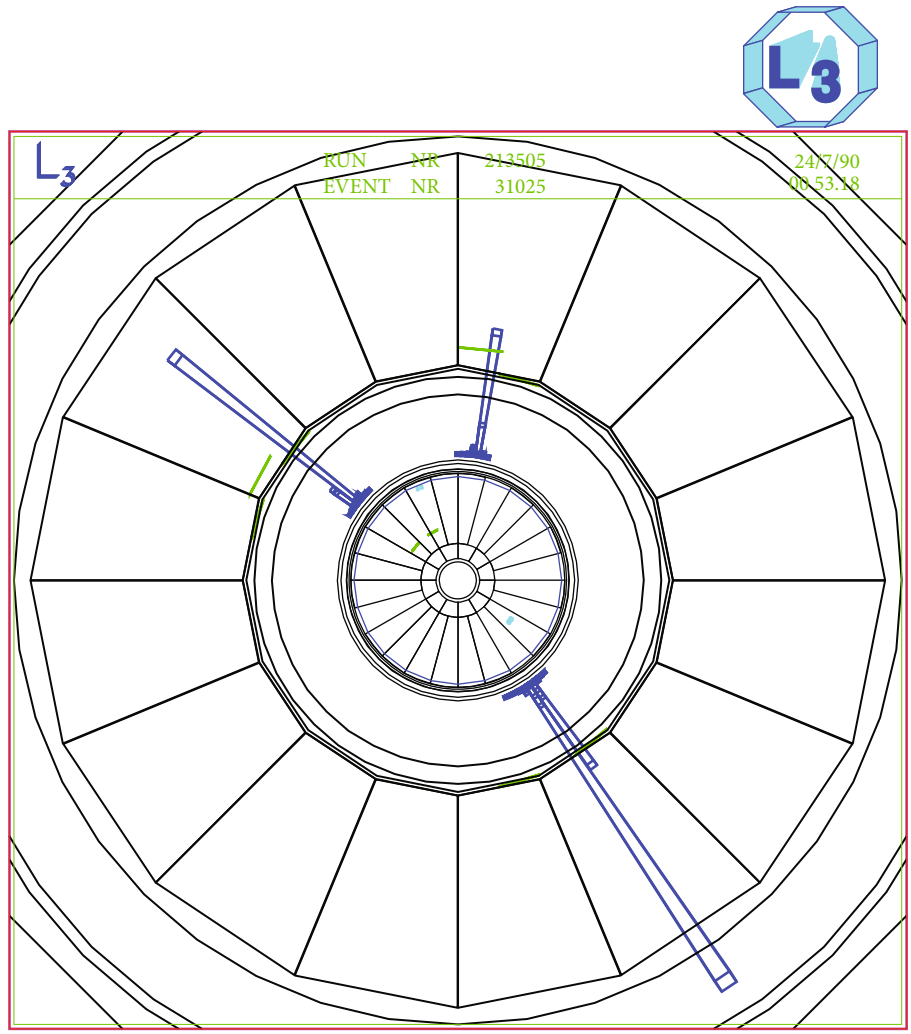

Figure 7: $e^+e^- \longrightarrow \gamma\gamma(\gamma)$ event in the L3 detector at CERN [88].

The coupling constant $g_n = \sqrt{4\pi}/\Lambda^{(n-4)}(n=6)$ is related to the mass scale Λ, $D_\mu = \partial_\mu - ieA_\mu$ is the QED covariant derivative, and $\tilde{F}^{\mu\nu}$ is the dual of the electromagnetic tensor $\tilde{F}^{\alpha\beta} = 1/2\varepsilon^{\alpha\beta\mu\nu}F_{\mu\nu}$. The differential cross section corresponds to $\mathscr{L}_6$ is shown in

$$\left(\frac{d\sigma}{d\Omega}\right)_T = \left(\frac{d\sigma}{d\Omega}\right)_{\text{QED}} [1+\delta_{\text{new}}] = \left(\frac{d\sigma}{d\Omega}\right)_{\text{QED}} \left[1 + \frac{s^2}{2\alpha}\left(\frac{1}{\Lambda^4} + \frac{1}{\tilde{\Lambda}^4}\right)(1-\cos^2\theta)\right]. \tag{20}$$

We use $\Lambda = \tilde{\Lambda} = \Lambda_6$, and higher order terms like Λ_7 or Λ_8 of δ_{new} are omitted.

To search for a deviation of QED, it is common to use χ^2 tests. This test compares the QED cross section to the experimental measured cross section. In the test, the QED cross section is modified by a non-QED direct contact term threshold energy scale Λ after equation (20). If the χ^2 test indicates a minimum of a finite threshold energy scale Λ, the energy of the cutoff parameter, it defines via the two equations $\Lambda = E = \hbar \times \nu$ and $\nu \times \lambda = c$ a finite size of the area where the e^+e^- annihilation must occur. For $\lambda = r_e$, this is a measure for size of the electron shown in (21), where $\hbar$ is the Planck constant and c is the speed of light.

$$r_e = \frac{\hbar c}{\Lambda}. \tag{21}$$

Equation (21) is generic, the calculation using the generalized uncertainty principle generates the same equation. It is interesting to notice that in equation (21) for $\Lambda \longrightarrow \infty$, the size of the object will be $r_e \longrightarrow 0$. In consequence, the point-like QED would be correct to infinite energies.

3. The Measurement of the Total Cross Section σ_{tot}

The $e^+e^- \longrightarrow \gamma\gamma(\gamma)$ reaction initiates in a storage of e^+e^- ring accelerators; it is a very clean signal in the detector. For example, Figure 7 shows an event from LEP in the L3

detector. Shown are the position and energy storage of an $e^+e^- \longrightarrow \gamma\gamma(\gamma)$ event perpendicular to the e^+e^- beam axis in the electromagnetic BGO calorimeter. The charge sensitive detectors of the inner trackers, the outer hadron calorimeter, and the muon chambers are free of any signal.

The total cross section can be described as a function of the number of events N in an angular range of the scattering angle $0 < |\cos\theta| < |\cos\theta|_{\max}$, the luminosity L, and the efficiency ε of the detector for $e^+e^- \longrightarrow \gamma\gamma$ events.

$$\sigma_{\text{tot}} = \frac{N}{\varepsilon L}. \tag{22}$$

All seven collaborations measured the total cross section σ_{tot} at different energies $\sqrt{s}$. To perform a total χ^2 fit of all experimental data, a model is needed to sum over all the information together in one total cross section at one $\sqrt{s}$. According to Table 11 in Appendix C, seventeen data sets exist from $\sqrt{s} = 55\,\text{GeV}$ to $207\,\text{GeV}$. Table 11 shows the luminosities and the references that the total cross section is published. At LEP, nine data sets exist measuring σ_{tot} from more than one detector. For the eight data sets, only one detector has measured σ_{tot}. A total χ^2 test would have in total 17 degrees of freedom, and if more than one detector is involved in one energy $\sqrt{s}$, the statistical error $\Delta\sigma(\text{stat})$ would decrease.

All the detectors of the six collaborations use different scattering angles $0 < |\cos\theta| < |\cos\theta|_{\max}$, luminosities L, and efficiencies ε for the $e^+e^- \longrightarrow \gamma\gamma$ events. In common, all the collaborations used for χ^2 tests the CERNLIB program MINUIT [89, 90] or Monte Carlo programs using the same radiative correction as discussed in Figures 3 and 4. The Monte Carlo program generates event number including different scattering angle ranges $0 < |\cos\theta| < |\cos\theta|_{\max}$ and efficiency ε. This fact allows to normalize the experimental data of the six collaborations to an imaginary L3 detector using the QED cross section of the different collaborations.

3.1. Calculation of $\sigma(tot)$, $\Delta\sigma(stat)$, Ratio $R(\exp)$, and $\Delta R(stat)$ for More than One Detector. At LEP, nine data sets exist measuring σ_{tot} from more than one detector. To calculate the total experimental cross section $\sigma(\exp)_{\text{tot}}^{(\text{sum})}$ (26), the statistical error $\Delta\sigma(\exp)_{\text{tot}}^{(\text{sum})}$ (27), the ratio $R(\exp) = R^{\text{sum}}$ (28), and the statistical error of this ratio $\Delta R(\text{stat}) = \Delta R(\text{stat})^{(\text{sum})}$ (30), the following input parameters are needed: the total experimental cross section $\sigma(\exp)_{\text{tot}}^{(\text{det}_i)}$ (pb) from VENUS, TOPAS, ALEPH, DELPHI, OPAL, and total L3-$N(\exp)$ event rate from Table 9 in Appendix C; the total QED cross section $\sigma(\text{QED})_{\text{tot}}^{(\text{det}_i)}$ (pb) from VENUS, TOPAS, ALEPH, DELPHI, OPAL, and total L3-$N(\text{QED})^{\text{L3}}$ event rate from Table 10 in Appendix C; and the luminosity used from the VENUS, TOPAS, ALEPH, DELPHI, L3, and OPAL experiment from Table 11 in Appendix C.

Under this condition in a first step, the model normalizes the experimental total cross section of a detector$_i$ $\sigma(\exp)_{\text{tot}}^{(\text{det}_i)}$ at one energy $\sqrt{s}$ to the L3 normalized experimental total cross section $\sigma(\exp)_{\text{tot}}^{(\text{L3}-\text{det}_i)}$ (23) via the total QED cross section of L3 $\sigma(\text{QED})_{\text{tot}}^{(\text{L3})}$ to the total QED cross section of the detector detector$_i$ $\sigma(\text{QED})_{\text{tot}}^{(\text{det}_i)}$ at $\sqrt{s}$ under investigation. For the detailed calculation, numerical values of $\sigma(\exp)_{\text{tot}}^{(\text{det}_i)}$ summarized in Table 9 (including the statistical error $\Delta\sigma(\exp)_{\text{tot}}^{(\text{det})}$) are needed.

The values of $\sigma(\text{QED})_{\text{tot}}^{(\text{det}_i)}$ are summarized in Table 10. The value of $\sigma(\text{QED})_{\text{tot}}^{(\text{L3})}$ is calculated via (17) and (18), and it is also added in Table 10 for simplicity.

Second, the model introduces a to-L3 QED normalized efficiency ε^{L3}, including the L3 QED event numbers $N(\text{QED})^{\text{L3}}$ of the total cross section at the $\sqrt{s}$ energy under investigation, the total QED cross section $\sigma(\text{QED})_{\text{tot}}^{(\text{L3})}$, and the L3 luminosity $L^{(\text{L3})}$ at $\sqrt{s}$ (24). The numerical values of $N(QED)^{L3}$ are taken from [64]. Inserted from this reference are the numbers from page 33 Table 1: "the expected 2γ events," which agrees with QED-Monte Carlo generators. The 3γ setup has been implicitly included in the generator with the parameter $p_{11} = \text{final} - \gamma - \text{state} = \text{gg}$ and $p_{55} = \text{accollinear} - \text{angle} - \text{acoll.} - \beta = 90.0$ (deg). The values for L3 luminosity $L^{(\text{L3})}$ at the $\sqrt{s}$ energy under investigation are taken from Table 11.

Third, the to-L3 normalized total QED cross section of the detector detector$_i$ $\sigma(\text{QED})_{\text{tot}}^{(\text{det}_i)}$ at $\sqrt{s}$ under investigation (23), the L3 QED efficiency ε^{L3} (24), and the luminosity of the different detectors $L_i^{(\text{det})}$ open the possibility to calculate the experimental counting rate of every detector normalized to L3 of this detector $N(\exp)_i^{\text{L3}}$ (25). The numerical values for $L_i^{(\text{det})}$ are summarized in Table 11. In this table, the important references for Tables 9 and 10 are included.

Including the detailed numerical numbers from (23)–(25), it is possible to sum over $N(\exp)_i^{\text{L3}}$ and $L_i^{(\text{det})}$ to calculate for every $\sqrt{s}$ under investigation the total summed cross section $\sigma(\exp)_{\text{tot}}^{(\text{sum})}$ (26) and the statistical error $\Delta\sigma(\exp)_{\text{tot}}^{(\text{sum})}$ (27).

The total summed cross section $\sigma(\exp)_{\text{tot}}^{(\text{sum})}$ (26) divided by the total QED cross section of L3 $\sigma(\text{QED})_{\text{tot}}^{(\text{L3})}$ allows to calculate the very important ratio R^{sum} at the $\sqrt{s}$ under investigation (28).

To calculate the statistical error $\Delta R(\text{stat})^{(\text{sum})}$ (30), the most conservative approach via the maximal possible error $\Delta\text{Max}R$ is used (29).

$$\sigma(\exp)_{\text{tot}}^{(\text{L3}-\text{det}_i)} = \sigma(\exp)_{\text{tot}}^{(\text{det}_i)} \frac{\sigma(\text{QED})_{\text{tot}}^{(\text{L3})}}{\sigma(\text{QED})_{\text{tot}}^{(\text{det}_i)}}, \tag{23}$$

Table 1: Summary of χ^2 test with BabaYaga@nlo generator.

	$(1/\Lambda)^4\,(\text{GeV}^{-4})$	σ	$(r \pm \Delta r) \times 10^{-17}\,(\text{cm})$
Direct	$(-1.62 \pm 0.83) \times 10^{-13}$	1.95	
p value	$(-1.62 \pm 0.83) \times 10^{-13}$	1.50	
$r \pm \Delta r$	$(-1.62 \pm 0.83) \times 10^{-13}$		1.25 ± 0.16

$$\varepsilon^{\mathrm{L3}} = \frac{N(\mathrm{QED})^{\mathrm{L3}}}{\left(\sigma(\mathrm{QED})_{\mathrm{tot}}^{(\mathrm{L3})} L^{(\mathrm{L3})}\right)}, \tag{24}$$

$$N(\exp)_i^{\mathrm{L3}} = \sigma(\exp)_{\mathrm{tot}}^{(\mathrm{L3-det}_i)} \varepsilon^{\mathrm{L3}} L_i^{(\mathrm{det})}, \tag{25}$$

$$\sigma(\exp)_{\mathrm{tot}}^{(\mathrm{sum})} = \frac{\sum_i N(\exp)_i^{\mathrm{L3}}}{\left[\varepsilon^{\mathrm{L3}} \sum_i L_i^{\mathrm{det}}\right]}, \tag{26}$$

$$\Delta\sigma(\exp)_{\mathrm{tot}}^{(\mathrm{sum})} = \frac{\sqrt{\sum_i N(\exp)_i^{\mathrm{L3}}}}{\left[\varepsilon^{L3} \sum_i L_i^{\mathrm{det}}\right]}, \tag{27}$$

$$R^{\mathrm{sum}} = \frac{\sigma(\exp)_{\mathrm{tot}}^{(\mathrm{sum})}}{\sigma(\mathrm{QED})_{\mathrm{tot}}^{(\mathrm{L3})}}, \tag{28}$$

$$\Delta\mathrm{Max}R = \frac{\sigma(\exp)_{\mathrm{tot}}^{\mathrm{sum}} + \Delta\sigma(\exp)_{\mathrm{tot}}^{\mathrm{sum}}}{\sigma(\mathrm{QED})_{\mathrm{tot}}^{\mathrm{L3}}}, \tag{29}$$

$$\Delta R(\mathrm{stat})^{(\mathrm{sum})} = \Delta\mathrm{Max}R - \mathrm{R}^{\mathrm{sum}}. \tag{30}$$

Not all different collaborations mark for $\sigma(\mathrm{QED})_{\mathrm{tot}}^{(\mathrm{det}_i)}$ a systematic error; for this reason, (27) and (30) include only the statistical error, which is dominating in this analysis. All collaborations generate with a Monte Carlo generator many millions of events to calculate the differential or total QED $e^+e^- \longrightarrow \gamma\gamma$ cross sections. This allows us to keep the systematic error originated from MC negligible, compared to the data statistical error. This analysis investigated one more possible important systematic error. We investigated two different Monte Carlo generators and used different energy ranges for the χ^2 test to study the systematic error. In the following sections, we will see that the interaction radius from all the four different tests are in the range of the statistical error the same (Table 2). It is interesting that even the completely independent analyses of different cross section agree with each other on this interaction radius (Table 2). It proves that the systematic error does not change the result of this analysis.

3.2. Calculation of $\sigma(tot)$, $\Delta\sigma(stat)$, Ratio $R(\exp)$, and $\Delta R($ stat$)$ for One Detector. The input data in the case only one detector contribute to the calculation of (31)–(35), and the detailed information is again included in Tables 9–11. In this case, eight data sets exist of σ_{tot} .

Under these conditions, the total experimental cross section normalized to L3 $\sigma(\exp)_{\mathrm{tot}}^{(\mathrm{single})}$ (31) is like (23), a function of the total experimental cross section of one detector $\sigma(\exp)_{\mathrm{tot}}^{\mathrm{det}}$ and the ratio of the total QED L3 cross section $\sigma(\mathrm{QED})_{\mathrm{tot}}^{\mathrm{L3}}$ to the total QED detector cross section $\sigma(\mathrm{QED})_{\mathrm{tot}}^{\mathrm{det}}$. It is similarly possible to calculate from the experimental error of detector $\Delta\sigma(\exp)_{\mathrm{tot}}^{\mathrm{det}}$ via the ratio $\sigma(\mathrm{QED})_{\mathrm{tot}}^{\mathrm{L3}}$ to $\sigma(\mathrm{QED})_{\mathrm{tot}}^{\mathrm{det}}$ the to-L3 normalized error $\Delta\sigma(\exp)_{\mathrm{tot}}^{(\mathrm{single})}$ (32). The ratio R^{single} (33) is a function of (31) and the total QED L3 cross section $\sigma(\mathrm{QED})_{\mathrm{tot}}^{\mathrm{L3}}$. The $\sigma(\mathrm{QED})_{\mathrm{tot}}^{\mathrm{L3}}$ cancels in (33), which replaces $\sigma(\exp)_{\mathrm{tot}}^{(\mathrm{single})}$ by $\sigma(\exp)_{\mathrm{tot}}^{\mathrm{det}}$ and $\sigma(\mathrm{QED})_{\mathrm{tot}}^{\mathrm{L3}}$ by $\sigma(\mathrm{QED})_{\mathrm{tot}}^{\mathrm{det}}$. To calculate the statistical error $\Delta R(\mathrm{stat})^{(\mathrm{single})}$ (35) for simplicity, the maximum value of $\Delta\mathrm{Max}R^{(\mathrm{single})}$ (34) is used to form the difference between $\Delta\mathrm{Max}R^{(\mathrm{single})}$ and R^{single}. The sum of (31) and (32) divided by $\sigma(\mathrm{QED})_{\mathrm{tot}}^{\mathrm{L3}}$ is shown in (34).

Table 2: Comparison of χ^2 tests total cross section to differential cross section.

Test	σ	Interaction radius ($r \pm \Delta r$)
4.1.1	1.95–1.50	$1.25 \pm 0.16 \times 10^{-17}$ (cm)
4.1.2	1.90–1.83	$1.44 \pm 0.20 \times 10^{-17}$ (cm)
4.1.4	1.81–1.80	$1.27 \pm 0.18 \times 10^{-17}$ (cm)
4.1.5	1.94–1.20	$1.17 \pm 0.15 \times 10^{-17}$ (cm)
Diff-cross	5.5	$1.57 \pm 0.07 \times 10^{-17}$ (cm)

Table 3: Summary $\sigma(\mathrm{tot})$, $\Delta\sigma(\mathrm{stat})$, ratio $R(\exp)$, and $\Delta R(\mathrm{stat})$.

$\sqrt{s}$ (GeV)	$\sigma(\mathrm{tot})\Delta\sigma(\mathrm{stat})$ (pb)	$R(\exp)\Delta R(\mathrm{stat})$
55	124.7 ± 13.2	0.92 ± 0.10
56	150.6 ± 9.7	1.15 ± 0.07
56.5	141.6 ± 22.9	1.10 ± 0.18
57	135.5 ± 10.8	1.07 ± 0.09
57.6	125.3 ± 2.0	1.01 ± 0.02
91	50.3 ± 0.9	0.99 ± 0.02
133	26.5 ± 5.8	1.10 ± 0.24
162	16.1 ± 2.4	0.98 ± 0.15
172	15.6 ± 2.6	1.08 ± 0.18
183	12.6 ± 0.3	0.99 ± 0.03
189	11.8 ± 0.2	0.99 ± 0.02
192	11.0 ± 0.5	0.95 ± 0.04
196	11.3 ± 0.3	1.02 ± 0.03
200	10.1 ± 0.3	0.95 ± 0.03
202	10.1 ± 0.4	0.97 ± 0.04
205	10.0 ± 0.3	0.99 ± 0.03
207	9.7 ± 0.2	0.98 ± 0.02

$$\sigma(\exp)_{\mathrm{tot}}^{(\mathrm{single})} = \sigma(\exp)_{\mathrm{tot}}^{\mathrm{det}} \frac{\sigma(\mathrm{QED})_{\mathrm{tot}}^{\mathrm{L3}}}{\sigma(\mathrm{QED})_{\mathrm{tot}}^{\mathrm{det}}}, \tag{31}$$

$$\Delta\sigma(\exp)_{\mathrm{tot}}^{(\mathrm{single})} = \Delta\sigma(\exp)_{\mathrm{tot}}^{\mathrm{det}} \frac{\sigma(\mathrm{QED})_{\mathrm{tot}}^{\mathrm{L3}}}{\sigma(\mathrm{QED})_{\mathrm{tot}}^{\mathrm{det}}}, \tag{32}$$

$$R^{\mathrm{single}} = \frac{\sigma(\exp)_{\mathrm{tot}}^{\mathrm{single}}}{\sigma(\mathrm{QED})_{\mathrm{tot}}^{\mathrm{L3}}} = \frac{\sigma(\exp)_{\mathrm{tot}}^{\mathrm{det}}}{\sigma(\mathrm{QED})_{\mathrm{tot}}^{\mathrm{det}}}, \tag{33}$$

$$\Delta\mathrm{Max}R^{(\mathrm{single})} = \frac{\sigma(\exp)_{\mathrm{tot}}^{\mathrm{single}} + \Delta\sigma(\exp)_{\mathrm{tot}}^{\mathrm{single}}}{\sigma(\mathrm{QED})_{\mathrm{tot}}^{\mathrm{L3}}}, \tag{34}$$

$$\Delta R(\mathrm{stat})^{(\mathrm{single})} = \Delta\mathrm{Max}R^{\mathrm{single}} - R^{\mathrm{single}}. \tag{35}$$

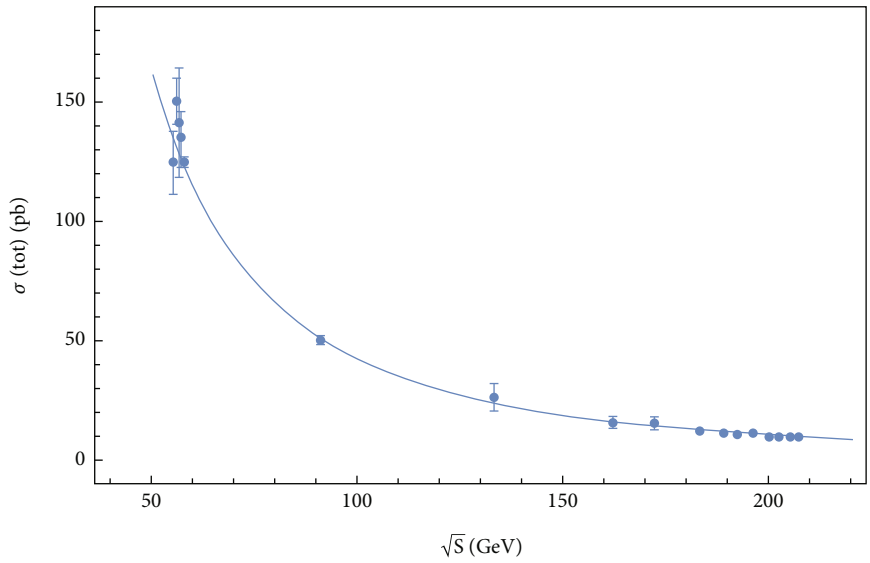

FIGURE 8: The $\sigma(\text{tot})$ of the $e^+e^- \longrightarrow \gamma\gamma(\gamma)$ reaction of all detectors as a function of center-of-mass energy $\sqrt{s}$. The data (points) are compared to QED prediction (solid line).

Not all different collaborations mark for $\sigma(\text{QED})_{\text{tot}}^{(\text{det})}$ a systematic error; for this reason, (32) and (34) include only the statistical error.

3.3. Numerical Calculation of $\sigma(tot)$, $\Delta\sigma(stat)$, Ratio $R(\text{exp})$, and $\Delta R(stat)$. Inserting the numerical values from Tables 9–11 in (23)–(35) allows to calculate $\sigma(\text{tot})$, $\Delta\sigma(\text{stat})$, ratio R (exp), and $\Delta R(\text{stat})$ shown in Table 3.

The $\sigma(\text{tot})$ values from $\sqrt{s} = 55\,\text{GeV}$ to 207 GeV together with $\Delta\sigma(\text{stat})$ of Table 3 compared to the total QED cross section $\sigma(\text{QED})_{\text{tot}}^{(\text{L3})}$ (17) is displayed in Figure 8.

Figure 8 shows a good agreement between the experimental measured values $\sigma(\text{tot})$ including the statistical error $\Delta\sigma(\text{stat})$ and the total QED cross section $\sigma(\text{QED})_{\text{tot}}^{(\text{L3})}$ in the range of sensitivity.

To search for deviation between measured values $\sigma(\text{tot})$ and the total QED cross section $\sigma(\text{QED})_{\text{tot}}^{(\text{L3})}$, the graphic of Figure 8 is not sensitive enough because the deviation is on the % level. A more sensitive graphic (Figure 9) is plotted to display the ratio $\sigma(\text{tot, meas.})/\sigma(\text{tot, QED})$ of the $e^+e^- \longrightarrow \gamma\gamma(\gamma)$ reaction of all detectors as a function of center-of-mass energy $\sqrt{s}$. In this plot, it is clearly seen that from $\sqrt{s} > 180\,\text{GeV}$, the ratio points are systematically under value 1.0, which means the data that measured total cross sections are systematically smaller than the QED predictions. The deviation is in general at % level and will be studied by the χ^2 test in the following sections.

In addition, it is also visible that the statistical errors for the 8 data points are much bigger than those for the 9 data points. The decrease of the statistical errors originated from the fact that at LEP, the nine data sets exist measuring σ_{tot} from more than one detector (27) and the eight data sets exist with that only one detector measuring σ_{tot}. For example, in the used model at $\sqrt{s} = 207\,\text{GeV}$, the statistical error is $\Delta\sigma(\text{stat}) = 0.2$ (pb), compared to the statistical error of L3 $\Delta\sigma(\text{stat}) = 0.34$ (pb) at the same $\sqrt{s} = 207\,\text{GeV}$ [64]. This is a decrease of approximately 42%.

4. Search for Finite Size of Electron Using a χ^2 Test of the Ratio $\sigma(\text{tot, meas.})/\sigma(\text{tot, QED})$

The signal for the finite size of the electron is weak, not visible in the graphic of the total experimental cross section compared with the QED total cross section in Figure 8. A deviation of approximately some % is visible in the graphic of the ratio $\sigma(\text{tot, meas.})/\sigma(\text{tot, QED})$ of the $e^+e^- \longrightarrow \gamma\gamma(\gamma)$ reaction in Figure 9. In accordance with the sensitivity between experiment and QED, a χ^2 test on this ratio (36) is performed to search for a minimum in χ^2.

$$\chi^2 = \sum_i \left\{ \frac{R(E_i\,;\text{exp}) - R(E_i\,;\text{QED}\,;\Lambda)}{\Delta R(E_i\,;\text{exp})} \right\}^2. \qquad (36)$$

The ratio of the experimental data $R(E_i\,;\text{exp})$ is in accordance with Table 3, the ratio of $\sigma(\text{tot, meas.})/\sigma(\text{tot, QED})$ at a $\sqrt{s}$ energy E_i. The statistical error $\Delta R(E_i\,;\text{exp})$ is the error at $\sqrt{s}$ energy E_i, in accordance with Table 3. The term to search for a deviation of a finite size of the electron is $R(E_i\,;\text{QED}\,;\Lambda)$ (37). The fit parameter $(1/\Lambda_6)^4$ is included, working as a function of the interaction size of the electron r_e (21).

$$R(E_i\,;\text{QED}\,;\Lambda) = \frac{\int_{\Omega_{\min}}^{\Omega_{\max}} (d\sigma/d\Omega)_{(E_i;\text{QED};\Lambda)}\, d\Omega}{\int_{\Omega_{\min}}^{\Omega_{\max}} (d\sigma/d\Omega)_{(E_i;\text{QED})}\, d\Omega}. \qquad (37)$$

It is essential for the whole program of the χ^2 test to use the fit parameter $(1/\Lambda_6)^4$ which is sensitive to the theoretical calculation for a deviation from the QED differential cross

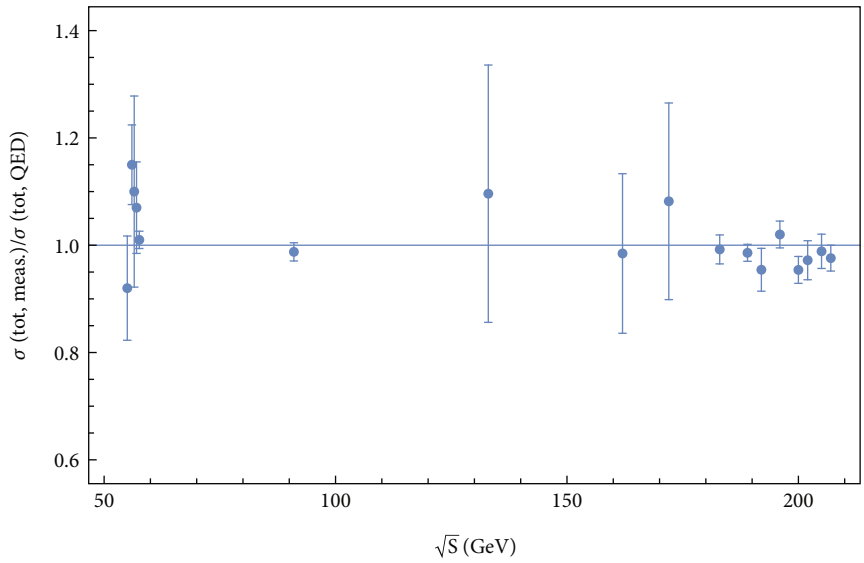

FIGURE 9: Ratio $\sigma(\text{tot, meas.})/\sigma(\text{tot, QED})$ of the $e^+e^- \longrightarrow \gamma\gamma(\gamma)$ reaction of all detectors as a function of center-of-mass energy $\sqrt{s}$. The experimental data (points) and QED prediction (solid blue line).

section for positive and negative interference. A parameter Λ_6 would test only the positive interference and cut out the negative part. This problem is visible in (37) and, in particular, (38). The parameter Λ_6 would keep the sign in front of $(1-\cos^2\theta)$ always positive independent of the $\pm$ sign from Λ_6. As a consequence, it always happens that $(d\sigma/d\Omega)_{(E_i;\text{QED};\Lambda)} > (d\sigma/d\Omega_{(E_i;\text{QED})})$ and $R(E_i\,;\text{QED}\,;\Lambda) > 1$. The χ^2 test would not be able to find values $R(E_i\,;\text{QED}\,;\Lambda) < 1$. For this reason, a negative interference could not be detected.

$$\int_{\Omega_{\min}}^{\Omega_{\max}} \left(\frac{d\sigma}{d\Omega}\right)_{(E_i;\text{QED};\Lambda)} d\Omega = \int_{\Omega_{\min}}^{\Omega_{\max}} \left[\left(\frac{d\sigma}{d\Omega}\right)_{(E_i;\text{QED})} \left(1 + \frac{s^2}{\alpha\Lambda_6^4}\left(1-\cos^2\theta\right)\right)\right] d\Omega. \tag{38}$$

The integrals ((37) and (38)) included the differential QED cross section $(d\sigma/d\Omega)_{(E_i;\text{QED})}$.

To test the angular contribution part of $R(E_i\,;\text{QED}\,;\Lambda)$ function, it is possible to integrate (37) over the $\sqrt{s}$ and use only the contribution of the angular distribution of the direct contact term (20) like

$$\begin{aligned} R(E_i\,;\text{QED}\,;\Lambda) &= \frac{\int_{\Omega_{\min}}^{\Omega_{\max}} (d\sigma/d\Omega)_{(E_i;\text{QED})} \left[1 + \left(s^2/\alpha\Lambda_6^4\right)\left(1-\cos^2\theta\right)\right] d\Omega}{\int_{\Omega_{\min}}^{\Omega^{\max}} (d\sigma/d\Omega)_{\left(E_{i\text{QED}}\right)} d\Omega} \\ &= \frac{k_1 \int_{\Omega_{\min}}^{\Omega^{\max}} \left[1 + \left(s^2/\alpha\Lambda_6^4\right)\left(1-\cos^2\theta\right)\right] d\Omega}{k_2 \int_{\Omega_{\min}}^{\Omega^{\max}} d\Omega}. \end{aligned} \tag{39}$$

The energy contribution to $R(E_i\,;\text{QED}\,;\Lambda)$ is in the range of % level, which opens the possibility to investigate the χ^2 test under the assumption that the constant k_1 equals approximately k_2.

4.1. Numerical Calculation of the χ^2 Tests. To investigate the sensitivity of the χ^2 test to the Monte Carlo generator BabaYaga@nlo [76] and the generator [73, 74], a separate numerical calculation for both tests was performed. In addition, an approximation was used to test only the impact of the direct contact term (20) in the χ^2 test.

The mathematical details of different possible calculation of significance and error of the interaction radius r are studied in Appendix D.

4.1.1. Calculation of the χ^2 Test with QED BabaYaga. The generators under discussion generate numbers of events respecting to L3 parameters (15). The events per angular range are used to fit a differential cross section as a function of $d\sigma/d\Omega[nb/s\text{rad}]$ and $|\cos\theta|$. An example of such a differential cross section is shown at $\sqrt{s} = 90.2\,\text{GeV}$ in Figure 5. The numerical parameters of this fit p_1 to p_6 defined in (14) for the 17 $\sqrt{s}$ energies from 55 GeV to 207 GeV are summarized in Table 8 (upper part). The χ^2 test on the ratio (36) as a function of $1/\Lambda^4$ for the $e^+e^- \longrightarrow \gamma\gamma(\gamma)$ reaction is displayed in Figure 10. The relevant center-of-mass energy ranges from $\sqrt{s} = 55\,\text{GeV}$ to 207 GeV, and the used QED predictions are from Monte Carlo generator BabaYaga@nlo.

The minimum of the χ^2 test including the error in Figure 10 is $1/\Lambda^4 = -1.62^{+0.84}_{-0.83} \times 10^{-13}\,\text{GeV}^{-4}$, which corresponds to $\Lambda = 1576 \pm 202\,\text{GeV}$. The χ^2 value at the minimum is $\chi^2 = 11.21$. The fit uses 17 degrees of freedom according to Table 3.

The important result of the χ^2 fit is that the fit parameter $1/\Lambda^4$ has a negative sign. According to Figure 9, the fit is sensitive to the fact that the total QED cross section is bigger than the experimental total cross section above approximately 180 GeV. The discussed direct contact interaction term δ_{new} (20) has a negative sign. This indicates a negative interference of the direct contact interaction in the $e^+e^- \longrightarrow \gamma\gamma$ reaction.

From the χ^2 fit results, the significance σ of the fit is essential. After international rules, the physic community

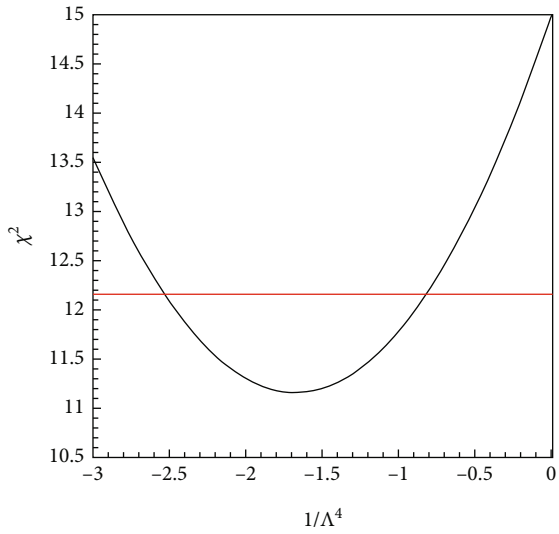

Figure 10: χ^2 test on the ratio (36) of the $e^+e^- \longrightarrow \gamma\gamma(\gamma)$ reaction from center-of-mass energy $\sqrt{s} = 55$ GeV to 207 GeV using QED data from Monte Carlo generator BabaYaga@nlo. The red line shows σ limit.

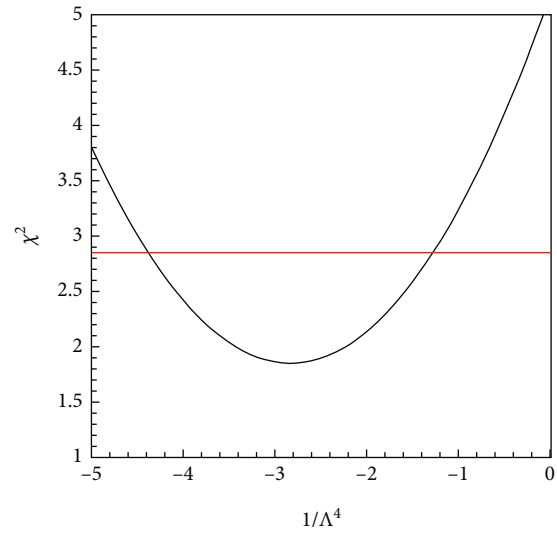

Figure 11: χ^2 test on the ratio (36) of the $e^+e^- \longrightarrow \gamma\gamma(\gamma)$ reaction from center-of-mass energy $\sqrt{s} = 91$ GeV to 207 GeV using QED data from Monte Carlo generator [73, 74]. The red line shows one σ limit.

accepts a $\sigma > 5$ as a discovery of new physics and a $\sigma < 5$ as a hint of new physics.

A detailed mathematical calculation of significance is discussed in Appendix D.1. A first approximation of the significance of the χ^2 fit can be directly estimated from the error bars of the fit $\sigma = A/\Delta A = 1.62/0.83 = 1.95$. In a second way to calculate the significance σ, a statistical probability function p (D.1) is used. The p value of the discussed χ^2 test for 17 degrees of freedom (with minimum $\chi^2 = 11.2$) is equal to $p = 0.15$. According to Figure 16, the significance is approximately $\sigma = 1.5$.

Similar to the significance, a detailed mathematical calculation of the error Δr_e of the interaction size r_e of the electron in the χ^2 test is discussed in the Appendix D.2. According to (21), the size of the interaction term is $r_e = 1.25 \times 10^{-17}$ (cm) and the error $\Delta r_e = 0.16 \times 10^{-17}$ (cm). The summary of all these results is given in Table 1.

4.1.2. Calculation of the χ^2 Test with QED Generator [73, 74]. The VENUS, TOPAS, OPAL, DELPHI, ALEPH, and L3 collaborations used for the QED cross section of the $e^+e^- \longrightarrow \gamma\gamma(\gamma)$ reaction and the generators [73, 74]. As discussed in Section 2.4.1, the deviation between BabaYaga and [73, 74] is approximately 0.9% under the condition that both generators used the same L3 parameters (15). Similar to the QED BabaYaga version, the events per angular range are used to fit a differential cross section as a function of $d\sigma/d\Omega$[pb/s rad] and $|\cos\Theta|$. The numerical parameters of this fit p_1 to p_6 are defined in (14) for the 7 $\sqrt{s}$ energies from 91.2 GeV to 200 GeV and summarized in the lower section of Table 8. Using QED predictions from Monte Carlo generator [73, 74], the χ^2 test on the ratio (36) as a function of $1/\Lambda^4$ for the $e^+e^- \longrightarrow \gamma\gamma(\gamma)$ reaction is displayed in Figure 11. The relevant center-of-mass energy ranges from $\sqrt{s} = 91.2$ GeV to 200 GeV.

Table 4: Summary of χ^2 test with generator [73, 74].

	$(1/\Lambda)^4$ (GeV^{-4})	σ	$(r \pm \Delta r) \times 10^{-17}$ (cm)
direct	$(-2.83 \pm 1.55) \times 10^{-13}$	1.83	
p - value	$(-2.83 \pm 1.55) \times 10^{-13}$	1.90	
$r \pm \Delta r$	$(-2.83 \pm 1.55) \times 10^{-13}$		1.44 ± 0.20

The minimum of the χ^2 test including the error in Figure 11 is $1/\Lambda^4 = -2.83^{+1.56}_{-1.55} \times 10^{-13}$ GeV^{-4}. The χ^2 value at the minimum is $\chi^2 = 1.85$. The fit uses 7 degrees of freedom.

Similar to the QED test with BabaYaga, $1/\Lambda^4$ in the QED test [73, 74] is negative. A first direct approximation of the significance is $\sigma = A/\Delta A = 2.83/1.55 = 1.83$. In a second approximation to calculate the significance σ, a statistical probability function p formula (D.1) is used. The p value of the discussed χ^2 test for 7 degrees of freedom (with minimum $\chi^2 = 1.85$) is equal to $p = 0.032$. Using Figure 16, this corresponds to a significance of approximately $\sigma = 1.9$.

According to (21), the size r of the interaction term is $(1.4) \times 10^{-17}$ (cm). The error Δr is $\Delta r = 0.20 \times 10^{-17}$ (cm) from equation (D.10). The summary of all these results is given in Table 4.

4.1.3. Numerical Calculation of the χ^2 Test Using Only Direct Contact Term. The χ^2 tests performed with the QED BabaYaga and [73, 74] generator request the calculation of the differential QED cross section and fit this data with (14).

Equation (39) opens the possibility to test straight the direct contact term (20). The deviation between the measured $R(\exp)$ and $R(\text{QED})$ is on the % level. This allows us to assume that the constant factors k_1 and k_2 are approximately the same, $k_1 \approx k_2$.

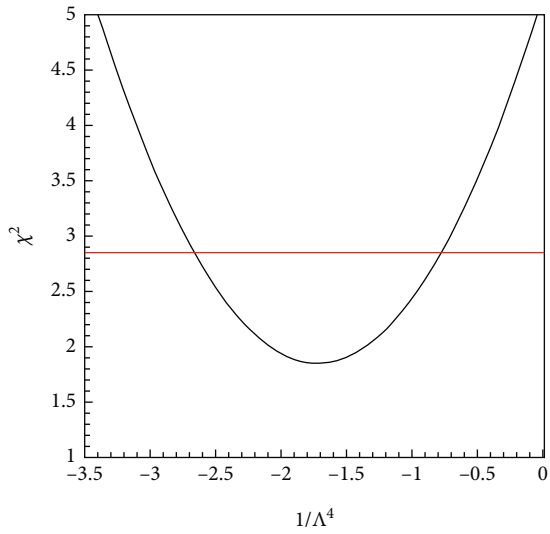

Figure 12: χ^2 test on the ratio (36) of the $e^+e^- \longrightarrow \gamma\gamma(\gamma)$ reaction from center-of-mass energy $\sqrt{s} = 91.2\,\text{GeV}$ to $200\,\text{GeV}$ using 7 degrees of freedom in the $k_1 \approx k_2$ approximation. The red line shows one σ limit.

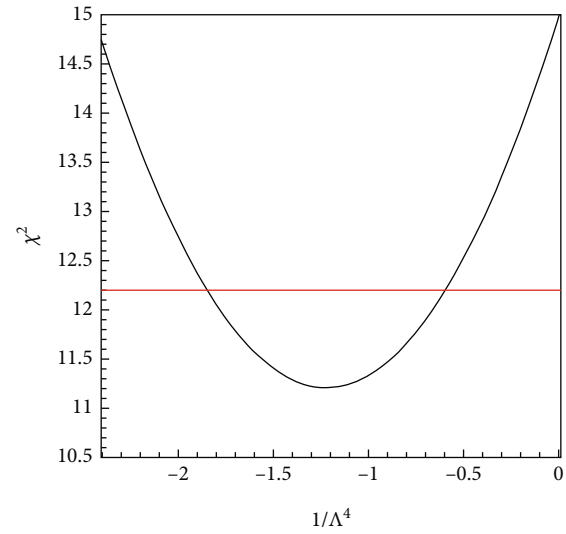

Figure 13: χ^2 test on the ratio (36) of the $e^+e^- \longrightarrow \gamma\gamma(\gamma)$ reaction from center-of-mass energy $\sqrt{s} = 52\,\text{GeV}$ to $207\,\text{GeV}$ using 17 degrees of freedom in the $k_1 \approx k_2$ approximation. The red line shows one σ limit.

Table 5: Summary of χ^2 test with 7 degrees of freedom in $k_1 \approx k_2$ approximation.

	$(1/\Lambda)^4$ (GeV^{-4})	σ	$(r \pm \Delta r) \times 10^{-17}$ (cm)
Direct	$(-1.72 \pm 0.95) \times 10^{-13}$	1.81	
p value	$(-1.72 \pm 0.95) \times 10^{-13}$	1.80	
$r \pm \Delta r$	$(-1.72 \pm 0.95) \times 10^{-13}$		1.27 ± 0.18

Table 6: Summary of χ^2 test with 17 degrees of freedom in $k_1 \approx k_2$ approximation.

	$(1/\Lambda)^4$ (GeV^{-4})	σ	$(r \pm \Delta r) \times 10^{-17}$ (cm)
Direct	$(-1.22 \pm 0.63) \times 10^{-13}$	1.94	
p value	$(-1.22 \pm 0.63) \times 10^{-13}$	1.20	
$r \pm \Delta r$	$(-1.22 \pm 0.63) \times 10^{-13}$		1.17 ± 0.15

According to Table 8, two $R(\text{QED})$ data sets exist with 7 degrees of freedom from $\sqrt{s} = 91.2\,\text{GeV}$ to $200\,\text{GeV}$ and 17 degrees of freedom from $\sqrt{s} = 55\,\text{GeV}$ to $207\,\text{GeV}$. Both data sets are tested.

4.1.4. Numerical Calculation of the χ^2 Test with 7 Degrees of Freedom in $k_1 \approx k_2$ Approximation. The χ^2 test on the ratio (36) as a function of $1/\Lambda^4$ for the $e^+e^- \longrightarrow \gamma\gamma(\gamma)$ reaction from center-of-mass energy $\sqrt{s} = 91.2\,\text{GeV}$ to $200\,\text{GeV}$ is displayed in Figure 12.

Inserted are the 7 $\sqrt{s}$ energies from Table 8 (lower part) and the relevant $R(\text{exp})$ parameters in Table 3, including also equations (36), (37), and (39) under the assumption $k_1 \approx k_2$.

The minimum of the χ^2 test including the error in Figure 12 is $1/\Lambda^4 = -1.72^{+0.94}_{-0.95} \times 10^{-13}\text{GeV}^{-4}$. The χ^2 value at the minimum is $\chi^2 = 1.85$. The fit uses 7 degrees of freedom.

Similar to the QED test BabaYaga and [73, 74], $1/\Lambda^4$ in this approximation is also negative. A first direct approximation of the significance is $\sigma = A/\Delta A = 2.83/1.55 = 1.81$. In a second approximation to calculate the significance σ, a statistical probability function p (D.1) is used. The p value of the discussed χ^2 for 7 degrees of freedom (with minimum $\chi^2 = 1.85$) is equal to $p = 0.032$. Using Figure 16, this corresponds to a significance of approximately $\sigma = 1.8$.

Table 7: Summary of the numerical calculation of the χ^2 tests.

Test	σ	Interaction radius $(r \pm \Delta r)$
4.1.1	1.95–1.50	$1.25 \pm 0.16 \times 10^{-17}$ (cm)
4.1.2	1.90–1.83	$1.44 \pm 0.20 \times 10^{-17}$ (cm)
4.1.4	1.81–1.80	$1.27 \pm 0.18 \times 10^{-17}$ (cm)
4.1.5	1.94–1.20	$1.17 \pm 0.15 \times 10^{-17}$ (cm)

According to (21), the size r of the interaction term is $(1.27) \times 10^{-17}$ (cm). The error Δr is after equation (D.10) $\Delta r = 0.18 \times 10^{-17}$ (cm). The summary of all these results is given in Table 5

4.1.5. Numerical Calculation of the χ^2 Test with 17 Degrees of Freedom in $k_1 \approx k_2$ Approximation. The χ^2 test on the ratio (36) as a function of $1/\Lambda^4$ for the $e^+e^- \longrightarrow \gamma\gamma(\gamma)$ reaction from center-of-mass energy $\sqrt{s} = 55\,\text{GeV}$ to $207\,\text{GeV}$ is displayed in Figure 13. Inserted in the χ^2 test are 17 $\sqrt{s}$ energies of $R(\text{exp})$ parameters of Table 3, including also equations (36), (37), and (39) under the assumption $k_1 \approx k_2$.

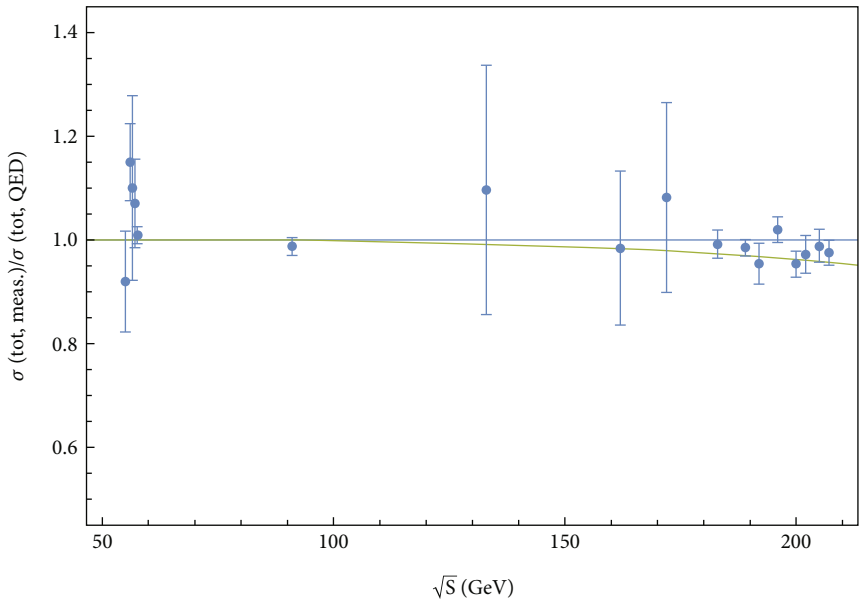

FIGURE 14: Ratio $\sigma(\text{tot, meas.})/\sigma(\text{tot, QED})$ of the $e^+e^- \longrightarrow \gamma\gamma(\gamma)$ reaction of all detectors as a function of center-of-mass energy $\sqrt{s}$. The experimental data (points), QED prediction (solid blue line), and green solid line χ^2 fit result of finite size of electron.

The minimum of the χ^2 test including the error in Figure 13 is $1/\Lambda^4 = -1.22^{+0.63}_{-0.63} \times 10^{-13}\,\text{GeV}^{-4}$. The χ^2 value at the minimum is $\chi^2 = 11.2$. The fit uses 17 degrees of freedom.

Similar to the QED test BabaYaga and [73, 74], $1/\Lambda^4$ is also negative in this approximation. A first direct approximation of the significance is $\sigma = A/\Delta A = 1.22/0.63 = 1.94$. In a second approximation to calculate the significance σ, a statistical probability function p (D.1) is used. The p value of the discussed χ^2 test for 17 degrees of freedom (with minimum $\chi^2 = 11.2$) is equal to $p = 0.15$. Using Figure 16, this corresponds to a significance of approximately $\sigma = 1.2$.

According to (21), the size r of the interaction term is $(1.17) \times 10^{-17}$ (cm). The error Δr is after equation (D.10) $\Delta r = 0.15 \times 10^{-17}$ (cm). The summary of all these results is given in Table 6.

4.2. Conclusion of the Four Different Numerical Calculations of the χ^2 Tests. The four χ^2 tests on the ratio (36) as a function of $1/\Lambda^4$ for the $e^+e^- \longrightarrow \gamma\gamma(\gamma)$ reaction from center-of-mass energy $\sqrt{s} = 55\,\text{GeV}$ to $207\,\text{GeV}$ are summarized in Table 7. The table contains test 4.1.1 (Calculation of the χ^2 Test with QED BabaYaga), test 4.1.2 (Calculation of the χ^2 Test with QED Generator [73, 74]), test 4.1.4 (Numerical Calculation of the χ^2 Test with 7 Degrees of Freedom in $k_1 \approx k_2$ Approximation), and test 4.1.5 (Numerical Calculation of the χ^2 Test with 17 Degrees of Freedom in $k_1 \approx k_2$ Approximation).

All the four different χ^2 tests show a minimum, including a negative $(1/\Lambda^4(\text{GeV}^{-4})$ value. This fact supports a negative interference effect of the direct contact term in Figure 2. Equation (20) has the term δ_{new} negative sign.

The sensitivities depend on the type of the χ^2 test and the methods of calculation. The direct calculated sensitivity

TABLE 8: The QED fit parameters p_1 to p_6 of the differential cross section from VENUS, TOPAS, ALEPH, DELPHI, and OPAL normalized to L3: upper part, BabaYaga; lower part, [73, 74].

GeV	p_1	p_2	p_3	p_4	p_5	p_6
55	-5.31	8.97	0.65	9.41	0.42	-7.30
56	-5.68	9.20	0.66	9.52	0.31	-7.09
56.5	-0.39	2.29	0.52	4.53	-1.28	-3.59
57	-6.81	9.55	0.65	9.81	-0.10	-6.05
57.6	-7.92	7.34	0.62	7.44	-0.98	-1.46
91.2	-9.28	9.08	0.61	9.90	-1.68	-2.06
133	-9.80	9.42	0.61	9.99	-1.63	-1.89
162	-4.02	6.29	0.58	8.95	-1.87	-4.74
172	-4.17	6.30	0.58	8.96	-2.13	-4.41
183	-4.42	6.57	0.59	9.11	-1.91	-4.60
189	-3.77	5.84	0.58	8.82	-2.83	-3.84
192	-4.89	6.81	0.59	9.27	-2.10	-4.27
196	-4.63	6.39	0.58	9.08	-2.37	-3.90
200	-4.29	6.44	0.59	9.07	-2.02	-4.56
202	-4.00	6.22	0.58	8.93	-2.03	-4.60
205	-4.11	6.27	0.58	8.98	-2.04	-4.55
207	-4.05	6.29	0.58	8.98	-1.95	-4.69
91.2	0.95	-0.34	0.08	1.16	-2.70	1.77
133	0.95	-0.31	0.09	1.19	-2.76	1.81
161	1.04	-0.34	0.13	0.69	-1.95	1.40
172	1.22	-0.47	0.18	-0.17	-0.62	0.75
183	1.27	-0.51	0.19	-0.37	-0.38	0.66
189	1.29	-0.52	0.20	-0.40	-0.41	0.70
200	1.29	-0.53	0.20	-0.40	-0.42	0.72

Table 9: The total experimental cross section $\sigma(\exp)_{\text{tot}}^{(\det_i)}$ (pb) from VENUS, TOPAS, ALEPH, DELPHI, OPAL, and total L3-$N(\exp)$ event rate.

GeV	VENUS	TOPAS	ALEPH	DELPHI	L3-$N(\exp)$	OPAL
55	46.4 ± 4.9					
56	55.8 ± 3.6					
56.5	52.5 ± 8.5					
57	50.2 ± 4.0					
57.6		50.2 ± 0.8				
91.2			45.13 ± 2.6	17.4 ± 0.8	1882	32.4 ± 2.3
133				9.42 ± 2.06		
162				5.76 ± 0.87		
172				5.55 ± 0.94		
183				4.27 ± 0.35	439	10.05 ± 0.43
189				4.27 ± 0.20	1302	8.79 ± 0.23
192				3.43 ± 0.43	193	9.24 ± 0.58
196				4.22 ± 0.28	555	8.43 ± 0.34
200				3.73 ± 0.25	424	7.39 ± 0.31
202				3.50 ± 0.34	223	7.88 ± 0.47
205					459	7.40 ± 0.31
207					863	6.78 ± 0.23

is for all χ^2 tests approximately stable, ranging from $\sigma = 1.95$ to $\sigma = 1.81$. The sensitivity calculations via the statistics of the p values range from $\sigma = 1.83$ to $\sigma = 1.20$. It is important to notice that the approximation of the k_1-k_2 method in χ^2 test is sensitive to the energy dependence of the k_1-k_2 factors. This dependence is not included in the χ^2 test and lowers the p values for large energy ranges, leading to a σ down to 1.20. Except the $\sigma = 1.20$, the range of sensitivities between the direct calculation and the exact calculation of σ values is approximately the same. No significant differences among Monte Carlo generator of BabaYage, the generator [73, 74], and the k_1-k_2 approximation could be detected.

The interaction radius $r \pm \Delta r$ is in the range of the statistical error Δr the same for all χ^2 tests. Table 7 summarizes all these information for the four χ^2 tests. In column 1, column 2, and column 3, the method, the range of σ, and the interaction radius $r \pm \Delta r$ are shown, respectively.

It is well known that statistical tests depend on the amount of data or degrees of freedom available. This number defines finally the significance σ. To test the differential cross section, every angular distribution bin of the differential cross section is one degree of freedom. For this reason, the test of the differential cross section has much higher degrees of freedom than the test of the total cross section of the same data set.

The USTC and ETHZ collaboration published [54, 91] a χ^2 test of the differential cross section of the $e^+e^- \longrightarrow \gamma\gamma(\gamma)$ reaction in year 2014. The measurements of the differential cross section of the $e^+e^- \longrightarrow \gamma\gamma(\gamma)$ reaction from the VENUS, TOPAS, OPAL, DELPHI, ALEPH, and L3 collaborations, collected between 1989 and 2003, are used to perform a χ^2 test to search for a finite size of an electron. Data exist between center-of-mass energy $\sqrt{s} = 55\,\text{GeV}$ to $207\,\text{GeV}$ at 17 $\sqrt{s}$. In [54, 91], Table 5 shows the χ^2 test of the differential cross section of the $e^+e^- \longrightarrow \gamma\gamma(\gamma)$ reaction. The 17 $\sqrt{s}$ energies contain 254 degrees of freedom.

It is interesting to notice that in [54, 91], the χ^2 test shows also a negative $(1/\Lambda)^4\,(\text{GeV}^{-4}) = -(4.05 \pm 0.73) \times 10^{-13}$ which is similar to the χ^2 tests in this study, but with a significance of $\sigma = 5.5$ [54, 91] (Table 2).

A comparison of the actual χ^2 test significance σ and the interaction radius r is shown in Table 2. To guide the eye, a copy of Table 7 is included. In the last line, results of the "diff-cross" from [54, 91] are also included.

The difference between the χ^2 tests of the total cross section and differential cross section is in the significance σ. It confirms that the test of the differential cross section including 257 degrees of freedom results in a higher σ as 17 degrees of freedom of the total cross section measurement. It is important to notice that the interaction radius $(r \pm \Delta r)$ is statistically the same for all tests.

5. Systematic Errors of χ^2 Test on the Total Cross Section

The default error in the ratio (36) $\Delta R(E_i\,;\exp\,;\text{sys})$ is usually the quadratic sum of the statistical error and systematic error, if both errors are independent. The data from the different groups show in the total cross section the statistical error. The systematic error was not published for every group in detail. Following the common manner of the different collaborations, only the statistical error $\Delta R(E_i\,;\exp)$ is used in (36).

Table 10: The total QED cross section $\sigma(\mathrm{QED})_{\mathrm{tot}}^{(\mathrm{det}_i)}$ (pb) from VENUS, TOPAS, ALEPH, DELPHI, OPAL, and total L3-$N(\mathrm{QED})^{\mathrm{L3}}$ event rate.

GeV	VENUS-L3$_{\mathrm{norm}}$	TOPAS-L3$_{\mathrm{norm}}$	ALEPH	DELPHI-L3$_{\mathrm{norm}}$	L3-$N(\mathrm{QED})^{\mathrm{L3}}$	OPAL
55	50.4-136					
56	48.5–131					
56.5	47.7–129					
57	46.9–127					
57.6		49.7-124				
91.2			42.8	18.3	50.9-1890	32.0
133				8.59-24.2		
162				5.85-16.3		
172				5.13-14.5		
183				4.57	12.7-457	9.32
189				4.28	11.9-1360	8.74
192				4.15	11.6–208	8.47
196				3.98	11.1–574	8.13
200				3.82	10.6–450	7.81
202				3.74	10.4–234	7.65
205					10.1–469	7.42
207					9.90-845	7.29

Table 11: The luminosity used from the VENUS, TOPAS, ALEPH, DELPHI, L3, and OPAL experiments plus references the total cross section is published.

GeV	VENUS	TOPAS	ALEPH	DELPHI	L3	OPAL
55	2.34 pb^{-1} [56]					
56	5.18 pb^{-1} [56]					
56.5	0.86 pb^{-1} [56]					
57	3.70 pb^{-1} [56]					
57.6		52.26 pb^{-1} [58]				
91			8.5 pb^{-1} [59]	36.9 pb^{-1} [60–62]	64.6 pb^{-1} [63]	7.2 pb^{-1} [57]
133				5.92 pb^{-1} [60–62]		
162				9.58 pb^{-1} [60–62]		
172				9.80 pb^{-1} [60–62]		
183				52.9 pb^{-1} [60–62]	54.8 pb^{-1} [64]	55.6 pb^{-1} [65]
189				151.9 pb^{-1} [60–62]	175.3 pb^{-1} [64]	181.1 pb^{-1} [65]
192				25.1 pb^{-1} [60–62]	28.8 pb^{-1} [64]	29.0 pb^{-1} [65]
196				76.1 pb^{-1} [60–62]	82.4 pb^{-1} [64]	75.9 pb^{-1} [65]
200				82.6 pb^{-1} [60–62]	67.5 pb^{-1} [64]	78.2 pb^{-1} [65]
202				40.1 pb^{-1} [60–62]	35.9 pb^{-1} [64]	36.8 pb^{-1} [65]
205					74.3 pb^{-1} [64]	79.2 pb^{-1} [65]
207					138.1 pb^{-1} [64]	136.5 pb^{-1} [65]

Systematic errors arise from the luminosity evaluation, the selection efficiency, the background evaluation, the choice of the QED-α^3 theoretical cross section as the reference cross section, the choice of the fit procedure, the type of the fit parameter, and the scattering angle in $|\cos\theta|$ for comparison between data and theoretical calculations.

In Table 3 and Figure 9, a small deviation from the $\sigma(\mathrm{QED})_{\mathrm{tot}}$ appears above $\sqrt{s} > 91.2\,\mathrm{GeV}$ in $R(\mathrm{exp})$. The

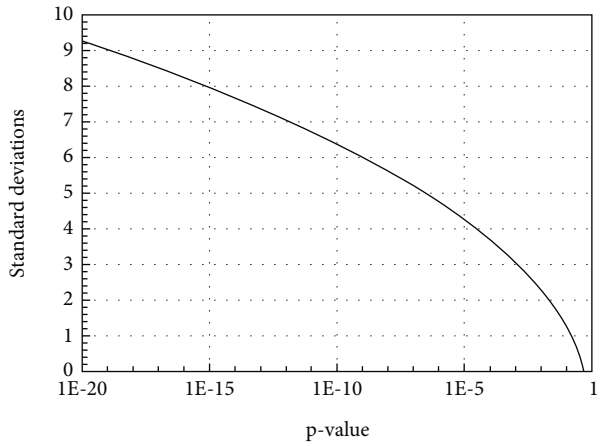

FIGURE 15: The p value (D.1) as a function of standard deviations $\mathrm{sg} = \sigma = 1$ to 10 (D.3).

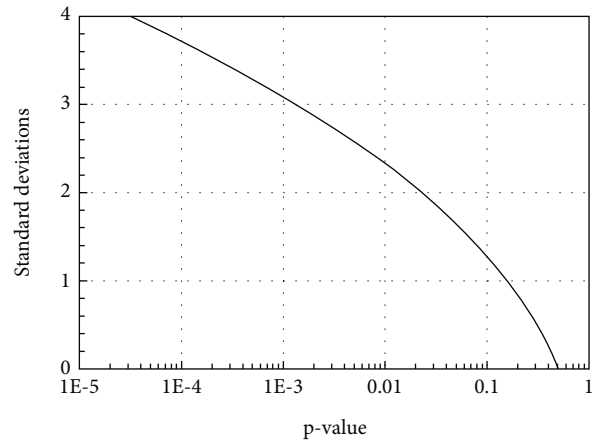

FIGURE 16: The p value (D.1) as a function of standard deviations $\mathrm{sg} = \sigma = 1$ to 4 (D.3).

systematic error of the measured total cross section of detector$_i$ $\sigma(\mathrm{exp})_{\mathrm{tot}}^{(\mathrm{det}_i)}$ and total QED cross section of $\sigma(\mathrm{QED})_{\mathrm{tot}}^{(\mathrm{det}_i)}$ above $\sqrt{s} > 91.2\,\mathrm{GeV}$ is for L3 [64] (Table 4) $0.10 < \Delta\sigma(\mathrm{meas.})_{\mathrm{sys}} < 0.13$ (pb) and $\Delta\sigma(\mathrm{QED})_{\mathrm{sys}} = 0.1$ (pb), for DELPHI [60–62] (Table 5, year 2000) $0.09 < \Delta\sigma(\mathrm{meas.})_{\mathrm{sys}} < 0.14$ (pb), and for OPAL [65] (Table 2) $0.05 < \Delta\sigma(\mathrm{meas.})_{\mathrm{sys}} < 0.08$ (pb). According to these tables, the $\Delta\sigma_{\mathrm{sys}}$ values behave statistically and the systematic error $\Delta\sigma(\mathrm{meas.})_{\mathrm{sys}}$ is much smaller than the statistical error $\Delta\sigma(\mathrm{meas.})_{\mathrm{sys}} < \Delta\sigma(\mathrm{meas.})_{\mathrm{stat}}$. No change as the function of the energy of the systematic errors above $\sqrt{s} > 91.2\,\mathrm{GeV}$ has been observed. The statistical behavior and the size of the $\Delta\sigma(\mathrm{meas.})_{\mathrm{sys}}$ exclude the possibility that the deviation of $R(\mathrm{exp})$ from $R(\mathrm{QED})$ could be originated from an energy $\sqrt{s}$ behavior of the systematic errors or the size of the error $\Delta\sigma(\mathrm{meas.})_{\mathrm{sys}}$.

6. Discussion

6.1. Ratio Plot of the Total Cross Section as a Function of the Finite Size of the Electron. The global χ^2 test under discussion uses the total cross section measured from different detectors. To investigate the deviation of the total measured $e^+e^- \longrightarrow \gamma\gamma(\gamma)$ cross section from QED total cross section, it is necessary to introduce an approach for a common total cross section in the energy range from $55\,\mathrm{GeV} < \sqrt{s} < 207\,\mathrm{GeV}$ shown in Figure 8. In a first view, the total measured cross section $\sigma(\mathrm{tot})$ and the QED cross section $\sigma(\mathrm{tot}, \mathrm{QED})$ is in a good agreement. To test in more detail the agreement between both cross sections, it is necessary to study the ratio $\sigma(\mathrm{tot}, \mathrm{meas.})/\sigma(\mathrm{tot}, \mathrm{QED})$ in Figure 9. To display the deviation from the ratio $\sigma(\mathrm{tot}, \mathrm{meas.})/\sigma(\mathrm{tot}, \mathrm{QED})$ in Figure 9, it is possible to calculate the ratio $R(\Lambda_6) = \sigma(\mathrm{QED})_{\mathrm{tot}}^{\mathrm{L3}}/\sigma(\mathrm{QED} + \Lambda_{\mathrm{top}})_{\mathrm{tot}}^{\mathrm{L3}}$. This ratio is calculated from the Monte Carlo generator, using the pure QED Λ_6 from the total cross section, in the minimum of the χ^2 test. The green line in Figure 14 displays the effect of a finite size of the electron generated from the χ^2 test.

A deviation from $\sigma(\mathrm{tot}, \mathrm{meas.})/\sigma(\mathrm{tot}, \mathrm{QED}) < 1.0$ appears above $\sqrt{s} = 180.0\,\mathrm{GeV}$, indicating, as in the χ^2 test, a negative interference. These findings agree with the measurement from L3 [64] (Figure 2) and DELPHI [60–62] (2000, Figure 2) considering the large statistical error bars.

6.2. Finite Size of an Electron in Rest. If the electron has a finite extension, the search with the $e^+e^- \longrightarrow \gamma\gamma(\gamma)$ reaction at high energies is a competition between the Lorentz contraction of the object and the size of the object in rest. Including the Lorentz contraction at $\sqrt{s} = 207\,\mathrm{GeV}$, the electron interaction size in rest would be approximately 2.92×10^{-14} (m). For comparison, this size would be bigger than the charge radius of the proton 0.87×10^{-15} (m) in rest. Under these circumstances, it seems possible to speculate that a charge distribution inside this electron volume exists. The effective Lagrangian of (19) is electromagnetic. The annihilation of the $e^+e^- \longrightarrow \gamma\gamma(\gamma)$ reaction would test the long-range direct contact term to the charge distribution.

7. Conclusion

The total cross section of the $e^+e^- \longrightarrow \gamma\gamma(\gamma)$ reaction measured from the VENUS, TOPAS, OPAL, DELPHI, ALEPH, and L3 collaborations was used to test the QED through a global χ^2 fit. It was the first time that is possible to detect a deviation from QED using a direct contact term. In this study, energy scale factor Λ is introduced to parametrise the the deviation from QED.

Four different χ^2 tests are used to test the Λ parameter, which is finally transferred to a finite size on the interaction area of the $e^+e^- \longrightarrow \gamma\gamma(\gamma)$ reaction, in consequence the finite size of the electron. All the four different χ^2 tests show a minimum, including a negative $(1/\Lambda)^4\,(\mathrm{GeV}^{-4})$ value. This fact supports a negative interference effect of the direct contact term. The maximum of the direct calculated sensitivity is approximately $\sigma = 1.9$. The range of the sensitivity among all four different χ^2 tests is approximately the same. The interaction radius $r \pm \Delta r$ is statistically the same. The best

fit value of Λ is $1576 \pm 202\,\text{GeV}$, leading to a finite interaction length of $r_e = (1.25 \pm 0.16) \times 10^{-17}\,(\text{cm})$. These results agree with the conclusion derived from the χ^2 test of the differential cross section [92] displayed in Table 2. After a common interpretation, this could be a "hint" for an effect of new physics [7, 54, 55, 91].

Appendix

A. Virtual and Soft Radiative Corrections of the $e^+e^- \longrightarrow \gamma\gamma(\gamma)$ Cross Section

If the energy of the photons from initial state radiation (soft Bremsstrahlung) is too small for detection $k_3/|p_+| = k_0 << 1$, the reaction can be treated as 2-photon final state in

$$e^+(p_+) + e^-(p_-) \longrightarrow \gamma(k_1) + \gamma(k_2)). \tag{A.1}$$

The equation for $\delta_{\text{virtual}} + \delta_{\text{soft}}$ is in

$$\begin{aligned}\delta_{\text{soft}} + \delta_{\text{virtual}} = -\frac{\alpha}{\pi}\Bigg\{ & 2(1-2v)(\ln k_0 + v) + \frac{3}{2} - \frac{1}{3}\pi^2 \\ & + \frac{1}{2(1+\cos^2\theta)} \times \left[-4v^2\left(3-\cos^2\theta\right) - 8v\cos^2\theta\right. \\ & + 4uv\left(5 + 2\cos\theta + \cos^2\theta\right) + 4wv(5 - 2\cos\theta) \\ & + \cos^2\theta - u\left(5 - 6\cos\theta + \cos^2\theta\right) \\ & - w\left(5 + 6\cos\theta + \cos^2\right) - 2u^2\left(5 + 2\cos\theta + \cos^2\theta\right) \\ & \left. - 2w^2\left(5 - 2\cos\theta + \cos^2\theta\right)\right]\Bigg\},\end{aligned} \tag{A.2}$$

$$v = \frac{1}{2}\ln\left(\frac{s}{m_e^2}\right), \tag{A.3}$$

$$u = \frac{1}{2}\ln\left(\frac{2(e+\cos\theta)}{m^2}\right), \tag{A.4}$$

$$w = \frac{1}{2}\ln\left(\frac{2(e-\cos\theta)}{m^2}\right), \tag{A.5}$$

$$m = \frac{m_e}{|p_+|}. \tag{A.6}$$

The mass of the electron m_e is still included in this equation. The total cross section of the two γ final states is in

$$\sigma^{2\gamma} = \sigma_0 + \frac{2\alpha^3}{s}\left[2(2v-1)^2\ln k_0 + \frac{4}{3}v^3 + 3v^2 + \left(\frac{2}{3}\pi^2 - 6\right)v - \frac{1}{12}\pi^2\right]. \tag{A.7}$$

B. Hard Radiative Corrections of the $e^+e^- \longrightarrow \gamma\gamma(\gamma)$ Cross Section

The soft-Bremsstrahlung photon energy is limited by a value $k_3/|p_1| = k_0 \ll 1$. If the energy of the photons from initial state radiations is above k_0, the process is treated as 3-photon final states.

$$e^+(p_+) + e^-(p_-) \longrightarrow \gamma(k_1) + \gamma(k_2) + \gamma(k_3). \tag{B.1}$$

For the differential cross section of $e^+e^- \longrightarrow \gamma\gamma(\gamma)$, it is necessary to introduce two additional parameters in the phase space. The calculation in (B.2) is performed in the extreme relativistic limit [93].

$$\frac{d\sigma}{d\Gamma_{ijk}} = \frac{d\sigma}{d\Omega_i d\Omega_k dx_k} = \frac{\alpha^3}{8\pi^2 s} w_{ijk} F(i,j,k), \tag{B.2}$$

$$w_{ijk} = \frac{x_i x_k}{y(z_j)}, x_i = \frac{k_{i0}}{\left|\vec{p}_+\right|}, \tag{B.3}$$

$$y(z_j) = 2e - x_k + x_k z_j, \tag{B.4}$$

$$z_j = \cos\left(\alpha_{ik}\right), \tag{B.5}$$

$$x_l = \frac{E_l}{\left|\vec{p}_+\right|}, \tag{B.6}$$

$$F(i,j,k) = \sum_P \left[-2m^2\frac{k_j'}{k_k^2 k_i'} - 2m^2\frac{k_j}{k_k'^2 k_i} + \frac{2}{k_k k_k'}\left(\frac{k_j^2 + k_j'^2}{k_i k_i'}\right)\right] = \sum_P M(i,j,k). \tag{B.7}$$

α_{ik} is the angle between k_i and k_j. P binds all permutations of $i, j, k \in (1, 2, 3)$. The quantities k_i and k_i' are

$$k_i = x_i(e - \cos\left(\theta_i\right)), \tag{B.8}$$

$$k_i' = x_i(e + \cos\left(\theta_i\right)), \tag{B.9}$$

where θ_i is the angle between the momentum of the i-th photon and$|\vec{p}_+|$. The total $3 \times \gamma$ cross section is

$$\sigma^{3\gamma} = \frac{1}{3!}\int d\Gamma_{ijk}, i, j, k \in \{1, 2, 3\}. \tag{B.10}$$

The integral runs over all phase space: $k_0 < x_i < 1$.

The practical calculation (B.10) can be approximated by an analytical approach. The photons get sorted after energy, $E_{\gamma 1} \geq E_{\gamma 2} \geq E_{\gamma 3}$, where γ_1 and γ_2 are treated as annihilation photons and γ_3 as hard Bremsstrahlung photon. The total cross section after integrations is as follows [73, 74].

$$\sigma^{3\gamma} = \frac{2\alpha^3}{s}\left[3 - \left(\ln\frac{4}{m^2} - 1\right)^2(2\ln k_0 + 1)\right]. \tag{B.11}$$

C. Four Tables Needed for the Numerical Calculations of the χ^2 Test

To calculate the differential cross section (14) from the BabaYaga@nlo generator [73, 74, 76], the QED fit parameters p_1 to p_6 of the differential cross section from VENUS, TOPAS, ALEPH, DELPHI, and OPAL normalized to L3 are given in Table 8. The parameters are sorted after the 17 $\sqrt{s}$ energies from $\sqrt{s} = 55\,\text{GeV}$ to $207\,\text{GeV}$ for the

BabaYaga generator Table 8 (upper part) and the 7 $\sqrt{s}$ energies from $\sqrt{s} = 91.2\,\text{GeV}$ to 200 GeV for the generator [73, 74] Table 8 (lower part).

The total experimental cross section $\sigma(\exp)_{\text{tot}}^{(\det_i)}$ (pb) and the statistical error in pb from VENUS, TOPAS, ALEPH, DELPHI, OPAL, and total L3 event rate L3-$N(\exp)$ are shown in Table 9 sorted after 17 $\sqrt{s}$ energies from $\sqrt{s} = 55$ GeV to 207 GeV.

The total QED cross section $\sigma(\text{QED})_{\text{tot}}^{(\det_i)}$ (pb) from VENUS, TOPAS, ALEPH, DELPHI, OPAL, and L3 is shown in Table 10. Table 10 is sorted after the 17 $\sqrt{s}$ energies from $\sqrt{s} = 55\,\text{GeV}$ to 207 GeV. As discussed in Sections 3.1 and 3.2, the 17 lines of Table 10 include separate information if only one detector or more than one detector is involved in the calculation of the total QED cross section.

Only one detector is involved in the lines VENUS – L 3_{norm} from $\sqrt{s} = 55\,\text{GeV}$ to 57 GeV. The left side is the VENUS QED total cross section in pb, and the right side is the L3 normalized total cross section in pb. The same situation counts for TOPAS – L3_{norm} at $\sqrt{s} = 57.6\,\text{GeV}$ and DELPHI – $(\text{L3}_{\text{norm}})$ from $\sqrt{s} = 133\,\text{GeV}$ to 172 GeV. The left side is the QED total cross section in pb, and the right side is the L3 normalized total cross section in pb.

More than one detector is involved at $\sqrt{s} = 91.2\,\text{GeV}$ and from 183 GeV to 207 GeV. In this case, the QED total cross section from the detector in pb is recorded (not normalized to L3) with the exception of L3 – N_{QED}. Left side of the line shows the total QED cross section of L3, and right side shows the total event rate of the L3 at this $\sqrt{s}$ energy.

The luminosities used from the VENUS, TOPAS, ALEPH, DELPHI, L3, and OPAL experiments are shown in Table 11. Table 11 gives also the references where the values of luminosities are taken from. The same references are also used for Tables 9 and 10.

D. Equations for the Calculation of Significance and Errors of the χ^2 Test

Using the fit program Minuit [89, 90] nearby the minimum of the parameter Λ, an error $\Delta\Lambda$ is calculated. As shown in Figures 10–13, the program sets a limit (red line) which allows to set $\Delta\Lambda$ values. The crossing points of the χ^2 function with the red line give the size of $\Delta\Lambda$ on the $1/\Lambda^4$ axis. It is common to calculate the significance σ of a statistical test in a first approximation by dividing the value of a fit parameter A by the error bar of ΔA like $\sigma = A/\Delta A$.

In addition, it is possible to use statistic theory ([94, 95]) to calculate the significance σ. For the χ^2 test, a statistical function $f = (\text{number of degrees of freedom, minimum of the } \chi^2)$ is used to calculate a p value. This p value allows also to calculate the significance σ.

D.1. Equations for the Calculation of the Significance of a χ^2 Test. To calculate the statistical significance p of a χ^2 test, a statistical probability function of $f = (\text{number of degrees of freedom } (l), \text{minimum of the } \chi^2\ T_{\text{obs}})$ is used. The integral of this function f is integrated from $\chi^2 = 0$ to the minimum in $\chi^2 = T_{\text{obs}}$. Following reference [94], the p value $p = P(T < T_{obs}|l)$ is defined as

$$p = \int_0^{T_{\text{obs}}} d\chi^2 \frac{1}{2^{l/2}\Gamma(l/2)} e^{-\chi^2/2} \left(\chi^2\right)^{-1+l/2}. \tag{D.1}$$

The gamma function $\Gamma(\alpha)$ (D.2) includes the parameter $\alpha = l/2$ with l the degrees of freedom.

$$\Gamma(\alpha) = \int_0^{\infty} y^{\alpha-1} e^{-y} dy. \tag{D.2}$$

The p value is connected including the Erf function to the number of standard deviations σ. The parameter sg in (D.3) is $\text{sg} = \sigma$.

$$p = \frac{1 - \text{Erf}\left(\text{sg}/\sqrt{2}\right)}{2}. \tag{D.3}$$

In Figure 15, the function of the standard deviations between $\text{sg} = \sigma = 1$ to 10 via p value is displayed [94].

In Figure 16, the function of the standard deviations between $\text{sg} = \sigma = 1$ to 4 via p value is displayed [94].

D.2. The Radius r_e and the Error Δr_e of the Interaction Size of the Electron in the χ^2 Test. The minimum of the fit parameter $1/\Lambda^4$ in the χ^2 test is a measure of the interaction size r_e of the electron (21).

$$r_e = \frac{\hbar c}{\Lambda}. \tag{D.4}$$

The minimum in the χ^2 test is given in units $y = 1/\Lambda^4 = y.yy^{+\Delta y.yy}_{-\Delta y.yy} \times \text{GeV}^{-4}$. For example, in accordance with Figure 12, $y = 1/\Lambda^4 = -1.72^{+0.94}_{-0.95} \times 10^{-13}\,\text{GeV}^{-4}$. To develop the parameter Λ as a function of y in

$$\Lambda = \left(\frac{1}{y}\right)^{1/4} \tag{D.5}$$

and use (D.4) allows to calculate the size r_e of the interaction radius. In the discussed example, the interaction radius is $r_e = (1.271) \times 10^{-17}$ (cm).

The error propagation of Δr is calculated in

$$\Delta r = \hbar \times c \times \frac{dr}{d\Lambda} \times \Delta\Lambda = -\frac{\hbar \times c}{\Lambda^2} \times \Delta\Lambda. \tag{D.6}$$

In (D.6), $\hbar$ is the Planck constant, c is the velocity of light, Λ is the cutoff parameter from the χ^2 test, and $\Delta\Lambda$ is the error. The error calculation of the parameter Λ is not a linear function of the minimum in χ^2.

Using $y = 1/\Lambda^4$, we can calculate the error of y (Δy) in equation (D.7), the error of Λ ($\Delta\Lambda$) in equation (D.8), and the first differential quotient $dy/d\Lambda$ in equation (D.9). Finally, it is possible to calculate the error of $\Delta\Lambda$ in equation (D.10).

$$\Delta y = \frac{dy}{d\Lambda}\Delta\Lambda, \tag{D.7}$$

$$\Delta\Lambda = \frac{\Delta y}{(dy/d\Delta)}, \tag{D.8}$$

$$dy/d\Delta = -4\Lambda^{-5}, \tag{D.9}$$

$$\Delta\Lambda = -\frac{1}{4}\Delta y\Lambda^{5}. \tag{D.10}$$

In the discussed example in Figure 12, the error would be $\Delta\Lambda = 214.41$ (GeV). Inserting this value in (D.6) would result in a $\Delta r = 0.1755 \times 10^{-17}$ (cm).

D.3. Conclusion Equations for the Calculation of Significance and Errors of the χ^2 Test. Equations (D.1)–(D.3) give an overview to calculate the significance σ of the χ^2 test. The significance is including the middle of the ranges from $1.6 < \sigma < 1.9$, a hint of new physics. The error Δr_e of the interaction size of the electron in the χ^2 test is described in (D.6)–(D.10). It is interesting to notice that according to Table 2, two independent χ^2 tests of the differential cross section and the total cross section result in the same interaction radius r_e in the range of statistical error.

Data Availability

All the $e^+e^- \longrightarrow \gamma\gamma$ cross section data used in this analysis are from the public results at VENUS, TOPAS, ALEPH, DELPHI, L3, and OPAL. They are public and can be seen in Table 11 in the manuscript, and the corresponding paper references for these numbers can also be found in Table 11 (references [57–66] of this manuscript).

Conflicts of Interest

The authors declare that they have no conflicts of interest

Acknowledgments

We are very grateful to André Rubbia, Claude Becker, Xiaolian Wang, Ziping Zhang, and Zizong Xu for the many years of encouraging support to the project. In particular, we thank in memory of Hans Hofer and Hongfang Chen for their long time engagement in this experiment. We also want to thank ARXIV.ORG for presenting our study publicly [92].

References

[1] T. Padmanabhan, "Planck length as the lower bound to all physical length scales," *General Relativity and Gravitation*, vol. 17, no. 3, pp. 215–221, 1985.

[2] G. Veneziano, "A Stringy nature needs just two constants," *Europhysics Letters*, vol. 2, no. 3, pp. 199–204, 1986.

[3] D. J. Gross and P. E. Mende, "String theory beyond the Planck scale," *Nuclear Physics B*, vol. 303, no. 3, pp. 407–454, 1988.

[4] M. Maggiore, "A generalized uncertainty principle in quantum gravity," *Physics Letters B*, vol. 304, no. 1-2, pp. 65–69, 1993.

[5] C. Rovelli and L. Smolin, "Discreteness of area and volume in quantum gravity," *Nuclear Physics B*, vol. 442, no. 3, pp. 593–619, 1995.

[6] L. J. Garay, "Quantum gravity and minimum length," *International Journal of Modern Physics A*, vol. 10, no. 2, pp. 145–165, 1995.

[7] I. Dymnikova, "Image of the electron suggested by nonlinear electrodynamics coupled to gravity," *Particles*, vol. 4, no. 2, pp. 129–145, 2021.

[8] P. Bosso, S. Das, and V. Todorinov, "Quantum field theory with the generalized uncertainty principle II: quantum electrodynamics," *Annals of Physics*, vol. 424, article 168350, 2021.

[9] G. G. Luciano and L. Petruzziello, "Generalized uncertainty principle and its implications on geometric phases in quantum mechanics," *The European Physical Journal Plus*, vol. 136, no. 2, p. 179, 2021.

[10] A. Kempf, G. Mangano, and R. B. Mann, "Hilbert space representation of the minimal length uncertainty relation," *Physical Review D*, vol. 52, no. 2, pp. 1108–1118, 1995.

[11] A. Kempf and G. Mangano, "Minimal length uncertainty relation and ultraviolet regularization," *Physical Review D*, vol. 55, no. 12, pp. 7909–7920, 1997.

[12] A. Kempf, "Mode generating mechanism in inflation with a cutoff," *Physical Review D*, vol. 63, no. 8, article 083514, 2001.

[13] S. Hossenfelder, "Minimal length scale scenarios for quantum gravity," *Living Reviews in Relativity*, vol. 16, no. 1, p. 2, 2013.

[14] K. Nakamura and Particle Data Group, "Review of particle physics," *Journal of Physics G*, vol. 37, no. 7A, article 075021, 2010.

[15] M. Sprenger, P. Nicolini, and M. Bleicher, "Physics on the smallest scales: an introduction to minimal length phenomenology," *European Journal of Physics*, vol. 33, no. 4, pp. 853–862, 2012.

[16] S. Hossenfelder, M. Bleicher, S. Hofmann, J. Ruppert, S. Scherer, and H. Stöker, "Signatures in the Planck regime," *Physics Letters B*, vol. 575, no. 1-2, pp. 85–99, 2003.

[17] J. Frenkel, "Die Elektrodynamik des rotierenden Elektrons," *Zeitschrift für Physik*, vol. 37, no. 4-5, pp. 243–262, 1926.

[18] M. Mathisson, "Neue Mechanik materieller Systeme," *Acta Physica Polonica*, vol. 6, pp. 163–200, 1937.

[19] H. Hönl and A. Papapetrou, "Über die innere Bewegung des Elektrons. I," *Zeitschrift für Physik*, vol. 112, no. 9-10, pp. 512–540, 1939.

[20] H. J. Bhabha and A. C. Corben, "General classical theory of spinning particles in a Maxwell field," *Proceedings of the Royal Society of London. Series A. Mathematical and Physical Sciences*, vol. 178, no. 974, pp. 273–314, 1941.

[21] V. Bargman, L. Michel, and V. L. Telegdxi, "Precession of the polarization of particles moving in a homogeneous electromagnetic field," *Physical Review Letters*, vol. 2, no. 10, pp. 435-436, 1959.

[22] P. L. Nash, "A Lagrangian theory of the classical spinning electron," *Journal of Mathematical Physics*, vol. 25, no. 6, pp. 2104–2108, 1984.

[23] K. Yee and M. Bander, "Equations of motion for spinning particles in external electromagnetic and gravitational fields," *Physical Review D*, vol. 48, no. 6, pp. 2797–2799, 1993.

[24] J. Bolte and S. Keppeler, "Semiclassical form factor for chaotic systems with spin 1/2," *Journal of Physics A: Mathematical and General*, vol. 32, no. 50, pp. 8863–8880, 1999.

[25] V. V. Nesterenko, "Singular Lagrangians with higher derivatives," *Journal of Physics A*, vol. 22, no. 10, pp. 1673–1687, 1989.

[26] Y. A. Rylov, "Spin and wave function as attributes of ideal fluid," *Journal of Mathematical Physics*, vol. 40, no. 1, pp. 256–278, 1999.

[27] M. Rivas, *Kinematical Theory of Spinning Particles*, Kluwer, Dordrecht, 2002.

[28] M. Rivas, "The dynamical equation of the spinning electron," *Journal of Physics A*, vol. 36, no. 16, pp. 4703–4716, 2003.

[29] S. M. Kuzenko, S. L. Lyakhovich, and A. Y. Segal, "A geometric model of the arbitrary spin massive particle," *International Journal of Modern Physics A*, vol. 10, no. 10, pp. 1529–1552, 1995.

[30] A. Staruszkiewicz, "Fundamental relativistic rotator," *Acta Physica Polonica B*, vol. 1, pp. 109–112, 2008.

[31] V. Kassandrov, N. Markova, G. Schaefer, and A. Wipf, "On the model of a classical relativistic particle of constant and universal mass and spin," http://arxiv.org/abs/0902.3688.

[32] J. Weyssenhoff and A. Raabe, "Relativistic dynamics of spin-fluids and spin-particles," *Acta Physica Polonica B*, vol. 9, pp. 7–18, 1947.

[33] M. H. L. Pryce, "The mass-center in the restricted theory of relativity and its connexion with the quantum theory of elementary particles," *Proceedings of the Royal Society A*, vol. 195, pp. 62–81, 1948.

[34] C. N. Fleming, "Covariant position operators, spin, and locality," *Physical Review B*, vol. 137, no. 1B, pp. B188–B197, 1965.

[35] M. Pavšič, "Classical motion of membranes, strings and point particles with extrinsic curvature," *Physics Letters B*, vol. 205, no. 2-3, pp. 231–236, 1988.

[36] M. Pavsic, E. Recami, and W. A. Rodrigues Jr., "Spin and electron structure," *Physics Letters B*, vol. 318, no. 3, pp. 481–488, 1993.

[37] D. Singh and N. Mobed, "Effects of space-time curvature on spin-1/2 particle zitterbewegung," *Classical and Quantum Gravity*, vol. 26, article 185007, 2009.

[38] M. S. Plyushchay, "Canonical quantization and mass spectrum of relativistic particle analogue of relativistic string with rigidity," *Modern Physics Letters A*, vol. 3, no. 13, p. 1299, 1988.

[39] M. S. Plyushchay, "Relativistic massive particle with higher curvatures as a model for the description of bosons and fermions," *Physics Letters B*, vol. 235, no. 1-2, pp. 47–51, 1990.

[40] M. S. Plyushchay, "Relativistic zitterbewegung: the model of spinning particles without Grassmann variables," *Physics Letters B*, vol. 236, no. 3, pp. 291–297, 1990.

[41] M. S. Plyushchay, "Relativistic particle with arbitrary spin in a non-Grassmannian approach," *Physics Letters B*, vol. 248, no. 3-4, pp. 299–304, 1990.

[42] A. O. Barut and N. Zanghí, "Classical model of the Dirac electron," *Physical Review Letters*, vol. 52, no. 23, pp. 2009–2012, 1984.

[43] E. Schrödinger, "Über die kräftefreie Bewegung in der relativistischen Quantenmechanik," *Sonderausgabe aus den Sitzungsberichten der Preussischen Akademie der Wissenschaften*, vol. 24, pp. 418–428, 1930.

[44] M. Abraham, "Prinzipien der Dynamik des Electrons," *Annalen der Physik*, vol. 10, pp. 105–179, 1902.

[45] H. A. Lorentz, *Theory of Electrons*, Dover, New York, NY, USA, 2nd edition, 1952.

[46] P. A. M. Dirac, "An extensible model of the electron," *Proceedings of the Royal Society of London. Series A. Mathematical and Physical Sciences*, vol. 268, no. 1332, pp. 57–67, 1962.

[47] A. Burinskii, "Gravity vs. quantum theory: is electron really pointlike?," *Journal of Physics: Conference Series*, vol. 343, article 012019, 2012.

[48] I. Dymnikova, A. Hasan, J. Ulbricht, and J. Wu, "Testing the size of fundamental particles and selfgravitating objects," *Gravitation and Cosmology*, vol. 5, pp. 230–234, 1999.

[49] I. Dymnikova, A. Hasan, and J. Ulbricht, "Size of fundamental particles and selfgravitating particlelike structures with de Sitter core," http://arxiv.org/abs/hep-ph/9903526.

[50] I. Dymnikova, J. Ulbricht, and J. Zhao, "Limits on sizes of fundamental particles and on gravitational mass of a scalar," *AIP Conference Proceedings*, vol. 564, pp. 239–246, 2001.

[51] I. G. Dymnikova, A. Hasan, J. Ulbricht, and J. Zhao, "Limits on the sizes of fundamental particles and gravitational mass of the Higgs particle," *Gravitation and Cosmology*, vol. 7, pp. 122–130, 2001.

[52] I. Dymnikova, A. Sakharov, J. Ulbricht, and J. Zhao, "Putting non point-like behavior of fundamental particles to test," http://arxiv.org/abs/hep-ph/0111302.

[53] I. Dymnikova, A. Sakharov, and J. Ulbricht, "Minimal length scale in annihilation," http://arxiv.org/abs/0907.0629.

[54] I. Dymnikova, A. Sakharov, and J. Ulbricht, "Appearance of a minimal length in e^+e^- annihilation," *Advances in High Energy Physics*, vol. 2014, Article ID 707812, 9 pages, 2014.

[55] D. Bourilkov, "Hint for axial-vector contact interactions in the data on $e^+e^- \longrightarrow e^+e^-(\gamma)$ at center-of-mass energies 192-208 GeV," *Physical Review D*, vol. 64, no. 7, article R071701, 2001.

[56] VENUS collaboration, "Measurement of the differential cross sections of $e^+e^- \longrightarrow \gamma\gamma$ and $e^+e^- \longrightarrow \gamma\gamma\gamma$ at $\sqrt{s} = 55, 56, 56.5$ and 57 GeV and search for unstable photino pair production," *Zeitschrift fuer Physik, C*, vol. 45, no. 2, pp. 175–191, 1989.

[57] OPAL collaboration, "Measurement of the cross sections of the reactions $e^+e^- \longrightarrow \gamma\gamma$ and $e^+e^- \longrightarrow \gamma\gamma\gamma$ at LEP," *Physics Letters B*, vol. 257, p. 531, 1991.

[58] TOPAS collaboration, "Studies of $e^+e^- \longrightarrow \gamma\gamma$ and $e^+e^- \longrightarrow \gamma\gamma\gamma$ reactions," *Physics Letters B*, vol. 284, p. 144, 1992.

[59] ALEPH collaboration, "Search for new particles in Z decays using the ALEPH detector," *Physics Reports*, vol. 216, p. 253, 1992.

[60] DELPHI collaboration, "Measurement of the $e^+e^- \longrightarrow \gamma\gamma(\gamma)$ cross section at LEP energies," *Physics Letters B*, vol. 327, p. 386, 1994.

[61] DELPHI collaboration, "Measurement of the $e^+e^- \longrightarrow \gamma\gamma(\gamma)$ cross section at the LEP energies," *Physics Letters B*, vol. 433, p. 429, 1998.

[62] DELPHI collaboration, "Determination of the $e^+e^- \longrightarrow \gamma\gamma(\gamma)$ cross-section at center-of-mass energies ranging from 189 GeV to 202 GeV," *Physics Letters B*, vol. 491, p. 67, 2000.

[63] L3 collaboration, "Tests of QED at LEP energies using $e^+e^- \longrightarrow \gamma\gamma(\gamma)$ and $e^+e^- \longrightarrow \ell^+\ell^-\gamma\gamma$," *Physics Letters B*, vol. 353, p. 136, 1995.

[64] L3 collaboration, "Study of multiphoton final states and tests of QED in e^+e^- collisions at $\sqrt{s}$ up to 209 GeV," *Physics Letters B*, vol. 351, p. 28, 2002.

[65] OPAL collaboration, "Multi-photon production in e^+e^- collisions at $\sqrt{s}$ =181-209 GeV," *The European Physical Journal C-Particles and Fields*, vol. 26, p. 331, 2003.

[66] O. J. P. Eboli, A. A. Natale, and S. F. Novas, "Bounds on effective interaction from $e^+e^- \longrightarrow \gamma\gamma$ at LEP," *Physics Letters B*, vol. 271, p. 274, 1991.

[67] L3 collaboration, "A test of quantum electrodynamics in the reaction $e^+e^- \longrightarrow \gamma\gamma(\gamma)$," *Physics Letters B*, vol. 288, p. 404, 1992.

[68] L3 collaboration, "Observation of multiple hard photon final states at $\sqrt{s}$ =130-140 GeV at LEP," *Physics Letters B*, vol. 384, p. 323, 1996.

[69] L3 Collaboration, "Hard-photon production at $\sqrt{s}$ =161 and 172 GeV at LEP," *Physics Letters B*, vol. 413, p. 159, 1997.

[70] L3 Collaboration, "Hard-photon production and tests of QED at LEP," *Physics Letters B*, vol. 475, p. 198, 2000.

[71] A. Bajo, I. Dymnikova, A. Sakharov, E. Sanchez, J. Ulbricht, and J. Zhao, "QED test at LEP200 energies in the reaction $e^+e^- \longrightarrow \gamma\gamma(\gamma)$," *AIP conference proceedings*, vol. 564, p. 255, 2001.

[72] J. Fujimoto, M. Igarashi, and Y. Shimizu, "Radiative correction to $e^+e^- \longrightarrow \gamma\gamma$ in electroweak theory," *Progress of Theoretical Physics*, vol. 77, p. 118, 1987.

[73] F. A. Berends and R. Kleiss, "Distributions for electron-positron annihilation into two and three photons," *Nuclear Physics B*, vol. 186, no. 1, pp. 22–34, 1981.

[74] CALKUL Collaboration, "Multiple bremsstrahlung in gauge theories at high energies (IV). The process $e^+e^- \longrightarrow \gamma\gamma\gamma\gamma$," *Nuclear Physics B*, vol. 239, p. 395, 1984.

[75] F. A. Berends and R. Gastmans, "Hard photon corrections for $e^+e^- \longrightarrow \gamma\gamma$," *Nuclear Physics B*, vol. 61, p. 414, 1973.

[76] BabaYaga@NLOhttp://inspirehep.net/literature/1740483; http://www.pv.infn.it/hepcomplex/babayaga.html;EPJ Web of Conferences 218, 07004 (2019) *PhiPsi*.

[77] S. F. King and S. R. Sharpe, "Exotic CERN events from exotic color states," *Nuclear Physics B*, vol. 253, pp. 1–13, 1985.

[78] C. N. Leung, S. T. Love, and S. Rao, "Low-energy manifestations of a new interactions scale: operator analysis," *Zeitschrift für Physik C Particles and Fields*, vol. 31, p. 433, 1986.

[79] S. D. Drell and S. J. Parke, "Constrains on radiative Z_0 decays," *Physics Letters B*, vol. 53, p. 1993, 1984.

[80] D. A. Dicus and X. Tata, "Anomalous photon interaction," *Physics Letters B*, vol. 155, p. 103, 1985.

[81] D. A. Dicus, "New interactions and neutrino counting," *Physical Review D*, vol. 31, p. 2999, 1985.

[82] E. Isiksal, *No. 9479 Eidgenössische Technische Hochschule, [M.S. thesis]*, ETH Zürich, Zürich, Switzerland, 1991.

[83] J. B. Xe, *Chinese University of Science and Technology, [M.S. thesis]*, USTC Hefei, Anhui 230 029, China, 1992.

[84] M. Maolinbay, *No. 11028 Eidgenössische Technische Hochschule, [M.S. thesis]*, ETH Zürich, Zürich, Switzerland, 1995.

[85] J. Wu, *No. JX1612-477, Chinese University of Science and Technology, [M.S. thesis]*, USTC Hefei, Anhui 230 029, China, 1997.

[86] J. Zhao, *No. JX1612-647 Chinese University of Science and Technology, [M.S. thesis]*, USTC Hefei, Anhui 230 029, China, 2001.

[87] K. Academy, "Light: electromagnetic waves, the electromagnetic spectrum photons," https://www.khanacademy.org/science/physics/light-waves/introduction-to-light-waves/a/light-and-the-electromagnetic-spectrum.

[88] l3.web.cern.ch/l3/l3pictures/events/gammas.html.

[89] F. James and M. Roos, *MINUIT, Function Minimization, and Error Analysis*, Release 89.12j, CERN Program Library Entry D506, 1994.

[90] F. James and M. Roos, "Minuit-a system for function minimization and analysis of the parameter errors and correlations," *Computer Physics Communications*, vol. 10, p. 343, 1975.

[91] C.-H. Lin, J. Ulbricht, J. Wu, and J. Zhao, "Experimental and Theoretical Evidence for Extended Particle Models," 2010, http://arxiv.org/abs/1001.5374.

[92] Y. Chen, M. Liu, and J. Ulbricht, "Hint for a minimal interaction length in $e^+e^- \longrightarrow \gamma\gamma$ annihilation in total cross section of center-of-mass energies 55-207 GeV," http://arxiv.org/abs/2112.04767v2.

[93] F. Mandl and T. H. Skyrme, "The theory of the double Compton effect," *Proceedings of the Royal Society of London. Series A. Mathematical and Physical Sciences*, vol. 215, no. 1123, pp. 497–507, 1952.

[94] F. Beaujean and A. Caldwell, "A test statistic for weighted runs," http://arxiv.org/abs/1005.3233v2 [math.ST] 16 Jul 2010.

[95] M. Rouaud, "Probability, statistics and estimation: propagation of uncertainties in experimental measurement (PDF)," 2013, http://www.incertitudes.fr/book.pdf.